Morphological controls on ~~Hortonian~~ surface runoff: An interpretation of steady-state energy patterns, maximum power states and dissipation regimes within a thermodynamic framework

Samuel Schroers[1], Olivier Eiff[2], Axel Kleidon[3], Ulrike Scherer[4], Jan~~-~~ Wienhöfer[1], Erwin Zehe[1]

[1]Institute of Water Resources and River Basin Management, Karlsruhe Institute of Technology – KIT, Karlsruhe, Germany
[2]Institute for Hydromechanics, Karlsruhe Institute of Technology – KIT, Karlsruhe, Germany
[3]Max~~-~~ Planck Institute for ~~Biochemistry, Hans Knöll Str. 10, 07745~~Biogeochemistry, Jena, Germany
[4]Engler-Bunte-Institut, Water Chemistry and Water Technology – KIT, Karlsruhe, Germany

Correspondence to: S. Schroers (samuel.schroers@kit.edu)

Abstract. Recent ~~developments in hydrology have led to a new~~research explored an alternative energy-centred perspective on ~~runoff~~hydrological processes, extending beyond the classical ~~mass dynamics~~analysis of the catchments water ~~in a catchment. For instance~~balance. Particularly, stream flow ~~has~~ and the structure of river networks have been analysed in ~~a thermodynamic~~an energy-centred framework, which allows the incorporation of two additional physical laws ~~and enhances our~~ : 1) the conservation of energy and 2) that entropy of an isolated system cannot decrease (1st and 2nd law of thermodynamics). This is helpful for understanding the self-organized geometry of ~~catchments as~~river networks and open ~~environmental~~catchment systems~~. Related investigations suggested that energetic extremal principles might constrain hydrological processes, because the latter are associated with conversions and dissipation of free energy.~~ in general. Here we expand this ~~thermodynamic~~ perspective, by exploring how hillslope ~~structures at the macro- and microscale~~topography and the presence of rill networks control the free energy balance of ~~Hortonian overland flow. We put special emphasis on the transitions of surface runoff processes at the hillslope scale, as~~ surface runoff at the hillslope scale. Special emphasis is on the transitions between laminar, mixed and turbulent flow conditions of surface runoff, as they are associated with kinetic energy dissipation as well as with energy transfer to eroded sediments. Starting with a general thermodynamic framework, we analyse in a first step how typical topographic shapes of hillslopes ~~energetically behave distinctly~~, representing different ~~in comparison to fluvial systems. To this end, we develop a general theory of surface runoff and of the related conversion of geopotential energy gradients into other forms of energy, particularly kinetic energy as the driver of erosion and sediment transport. We then use this framework at a macroscopic scale to analyse how combinations of typical hillslopes profiles and width distributions~~morphological stages, control the spatial patterns of ~~steady-state stream power and~~ potential and kinetic energy of surface runoff and energy dissipation along the flow path~~. At the microscale, we analyse flow concentration in rills and its influence on the distribution of energy and dissipation in space. Therefore, we develop a new numerical method for the~~ during steady states. Interestingly, we find that a distinct maximum in potential energy of surface runoff emerges along the flow path, which separates upslope areas of downslope potential energy growth from downslope areas where potential energy declines. A comparison with associated erosion processes indicates that the location of this maximum depends on the relative influence of diffusive and advective flow and erosion processes. In a next step, we use this framework to analyse the energy balance of surface runoff observed during hillslope-scale rainfall simulation experiments, which provide separate measurements of flow velocities for rill- and for sheet flow. To this end, we calibrate the physically based hydrological model Catflow ~~model~~, which ~~allows a dynamical separation of Hortonian~~distributes total surface runoff between a rill- and a sheet flow domain~~. We calibrated the new Catflow-Rill model to rainfall simulation experiments and observed overland flow in the Weiherbach catchment and found evidence that flow accumulation in rills serves as a means to redistribute energy gradients in space, therefore minimizing energy expenditure along the flow path, while also maximizing overall power of the system. Our results indicate that laminar sheet flow and turbulent rill flow on hillslopes develop to a dynamic equilibrium that~~ , to these experiments and analyse the spatial patterns of potential energy, kinetic energy and dissipation. This reveals again the existence of a maximum of potential

Formatted: German (Germany)

energy in surface runoff as well as a connection to the relative contribution of advective and diffusive processes. In case of a strong rill flow component, the potential energy maximum is located close to the transition zone, where turbulence or at least mixed flow may emerge. Furthermore, the simulations indicate an almost equal partitioning of kinetic energy into the sheet and the rill flow component. When drawing the analogy to an electric circuit, this distribution of power and erosive forces to erode and transport sediment corresponds to a maximum power ~~state, and that the transition of flow from one domain into the other is marked by an energy maximum in space~~configuration.

1 Introduction

RunoffSurface runoff in rivers and from hillslopes is of key importance to biological, chemical, and geomorphological processes. Landscapes, habitats, and their functionalities are coupled to the short and long-term evolution of rainfall-runoff systems. As we live in a changing environment it has been of mayor interest to explain the development of runoff systems and how ecological (Zehe et al., 2010; Bejan and Lorente, 2010), chemical (Zhang and Savenije, 2018; Zehe et al., 2013) and geomorphological (Leopold and Langbein, 1962; Kirkby, 1971; Yang, 1971; Kleidon et al., 2013) processes organize in time and space in order to deplete the free energy provided by water flow. In this study. Here we direct our focus on the most apparent runoff, stream flow in river systems and subsequently energy balance of surface runoff on hillslopes.particularly at the hillslope scale using a thermodynamic framework. Typically, the momentum balance of surface runoff and its momentum balance are stream flow is strongly dominated by friction, which is usually characterized by frictionthe flow laws such as they are expressed by Daryof Darcy-Weißbach, Manning or Chezy (Nearing et al., 2017). Consequently, the estimations of hydraulic estimates of flow are bound tovelocities rely on the semi-empirical parameters of these laws, which in essence express the ability of a system to dissipate free energy to bound thermal energy via friction into heat and thus to produce entropy (Zehe and Sivapalan., 2009). The rate at which dissipation happens is determined by these parameters, which are primarily assumed to be constant coefficientsA thermodynamic perspective appears hence as the natural choice for given hydraulic conditions but often are used as calibration parameters in order to reproduce the observed values of a variable, such as flow velocities or water levels. Ourdeeper understanding of the how the mass, momentum and energy balances of surface runoff are controlled by and interact with the landscape, and how short and long-term feedbacks determine the co-development of complexform and functioning of hydrological systems, which include feedback loops between flow and its driving energy gradients is therefore incomplete if we do not include an additional principle or law that sheds light on dissipation (Paik and Kumar, 2010.; Singh, 2003).

1.1 Thermodynamics in landscape evolution and optimal channel networks

Leopold and Langbein (1962) were amongstamong the first to introduce thermodynamic principles in landscape evolution. Representing a one-dimensional river profile as a sequence of heat engines with ponyprony brakes, (see Fig. 1), they showed that the most likely distribution of potential energy per unit flow along a rivers course to the sea follows an exponential function. Their main hypothesis is the principle ofwas that stream flow performs least work, or equivalently, that the constant production of entropy per flow volume is constant. Yang (1976) extended this principle and termed it minimum stream power. He effectively and detailed how flow velocity, slope, depth and channel roughness of a stream should adjust in order to fulfil the hypothesis of minimum steamto minimize stream power. In his work about optimal stream junction angles, Howard (1990) also assumed that stream power is minimized, while Rodriguez-Iturbe et al. (1992) in their study about proposed that optimal drainage patterns deduced that drainagechannel networks (OCN) minimize overall energy dissipation. Therefore, theThe authors consideredpostulated three principles, which were also applied and tested in subsequent papers :(Rodriguez-Iturbe et al., 1994; Ijjaz Vasquez et al., 1993). These have been termed (1) the principle of minimum energy expenditure in any link of the network, (2) the principle of equal energy expenditure per unit area, and (3) the principle of minimum total energy expenditure in the entire network as a whole. Notably. Subsequent work of these authors (Rodriguez-Iturbe et al., 1994; Ijjaz Vasquez et al., 1993were able to show) revealed that by application of these principles they could produceyielded three-dimensional drainage networks that follow geometric laws observed in nature (accordance with Horton's lawlaws of stream number and Horton's law of stream lengths; Horton 1945 (Smart, 1972).

~~Closely related is~~ In climate research, Paltrigde (1979) proposed the principle of maximum entropy production ~~(Paltridge, 1979) which states~~. He showed that ~~driving energy gradients are depleted as fast as possible. This implies a maximization of~~ a simple two box model allowed a successful reproduction of the steady state temperature distribution on Earth, which maximizes entropy production, expressed as the product of the heat flow and ~~driving gradient, or stated differently, a maximization of the rate of free energy production und thus power (~~the driving temperature difference. Kleidon et al~~.~~, (2013~~).~~ Kleidon et al. (2013) argue)~~ argued that ~~while~~maximum entropy production in steady state is equivalent to a maximization of power, which means that the flow extracts free energy at a maximum rate from the driving potential energy gradient. The authors applied the maximum power principle to river systems and proposed that they develop to a state of maximum power in sediment flows: While the driving geopotential gradient is depleted at the maximum rate, the associated sediment export maximizes with the same rate. ~~The authors also analyse how the formation of structures (channels) enhances these dynamics and conclude that maximum power is in line with the preceding principle of minimization of frictional losses as transfer of energy to sediment maximizes and frictional dissipation of kinetic energy minimizes simultaneously.~~

~~Motivated by their similarity to river networks, several studies tested whether hillslope scale rill networks develop in accordance with the~~ Furthermore, the authors relate maximum power in the river network to minimum energy expenditure ~~theory of river systems~~, as minimum dissipation implies ~~(Gómez et al., 2003; Rieke-Zapp and Nearing, 2005; Berger et al., 2010).~~ ~~Indeed, Rieke-Zapp and Nearing (2005) as well as Gomez et al. (2003) found in their experiments that the development of rill networks on hillslope scale follows the same trend of minimization of energy expenditure as it was proposed for river networks (Ijjasz-Vaquez et al., 1993).~~ ~~However, in contrast to the analysis of the development of pure networks and their self-similar characteristics (Rodiguez-Iturbe et al., 1994), hillslope-scale analysis of thermodynamic principles must include the transitional emergence of rills as they do not exist a priori (Favis-Motlock et al., 2000). The common assumption here is~~ that ~~rill flow reduces the volume specific dissipative loss due to a larger hydraulic radius (Berkowitz and Zehe, 2020), which causes larger flow velocities compared to sheet flow. However, this assumption was not validated. The geometry and topology of these drainage networks are time-dependent, as a response to transient flows of water and sediments, and these networks~~a maximum of potential energy can be converted into kinetic energy of the water and sediment flux.

1.2 Surface runoff and hillslope morphology and the role of energy conversions

Though surface runoff on hillslopes is governed by the same physics as stream flow, there are also important differences. Overland flow is an intermittent threshold response to rainfall events (Zehe and Sivapalan, 2009) caused either by infiltration excess (Horton 1945, Beven 2004) or saturation excess (Dunne and Black, 1970). Surface runoff flows along a partially saturated soil and may hence either accumulate downslope or re-infiltrate. Downslope re-infiltration implies an export of water mass and thus potential energy into the soil (Zehe et al, 2013), and the related decline in flow depth reduces shear stress which affects the momentum balance. Overland flow is typically very shallow compared to the roughness elements, which makes the use of the above-mentioned flow laws even more challenging (Phelps, 1975), and it manifests either as diffusive sheet flow or advective flow in rill networks. Due to the transient nature of overland and sediment flows, rill networks are generally transient but they develop in a self-reinforcing manner (Gómez et al., 2003; Rieke-Zapp and Nearing, 2005; Berger et al., 2010).

Micro rills emerge at some critical downstream distance on the hillslope (cf. Horton's (1945) "belt of no erosion") and ~~usually~~ continue in parallel for some length before they merge into larger rills (Schumm et al., 1984). Sometimes ~~they~~these rills split apart ~~and can expand~~before converging into larger gullies (Achten et al., 2008; Faulkner, 2008) ~~before~~and finally ~~forming the~~connecting to a river channel. This transitional emergence of a structured drainage network was firstly stated in Playfair's Law (cited in Horton, 1945) and has since then been observed in a variety of studies (Emmett, 1970; Abrahams et al., 1994; Evans et al., 1995). Motivated by the similarity to river networks and surface rill networks, several experimental studies explored whether rill networks grow towards and develop as least energy structures in accordance with the theory of optimal channel networks (Gómez et al., 2003; Rieke-Zapp and Nearing, 2005; Berger et al., 2010). The studies of Rieke-Zapp and

Nearing (2005) and Gomez et al. (2003) revealed that the emergence of rill networks and their development implies indeed a reduction of energy expenditure, which has previously been shown for stream channel networks (Ijjasz-Vaquez et al., 1993). In line with these findings, Berkowitz and Zehe (2020) proposed that rill flow reduces the volume specific dissipative energy loss due to a larger hydraulic radius compared to sheet flow, which is equal to smaller rills merging into a larger as noted by Parsons et al. (1990).

The possible optimization of ~~hydraulic geometry~~river or ~~structure~~rill network geometries through the interplay of surface runoff, erosion and deposition of ~~soil and sediment~~soils/ sediments is ~~but one mechanism which works in~~ the first point that motivates an analysis from a thermodynamic ~~rainfall-runoff systems. In some of the most~~perspective. The second point relates to the transition from laminar to turbulent flow conditions, which was already corroborated by Emmet (1970) in a set of comprehensive field and laboratory experiments ~~which were dedicated to investigating~~to investigate hydraulics of overland flow~~, Emmett (1970) measured a transition from laminar to turbulent flow on hillslope plots of up to 12m downstream length. This suggests that the upslope~~. As laminar ~~runoff dissipates less~~flow converts more potential energy into kinetic energy per unit volume ~~and further downstream evolves to a more dissipative~~than turbulent flow ~~regime.~~, it is of interest whether and how this transition relates to the emergence of rills and their optimization. Parsons et al. (1990) measured the hydraulic properties of overland flow ~~hydraulic conditions~~ on a semiarid hillslope in Arizona and attributed ~~an~~the observed downslope decrease ~~of~~in the frictional flow resistance to the accumulation of surface flow in fewer, but larger rills~~, like~~. This is similar to a transition of inter-rill flow, from here onwards referred to as sheet flow (Dunne and Dietrich, 1980), to rill flow. More recently a concept emerged that upholds a theory of a slope-velocity equilibrium (Govers, 2000; Nearing et al., 2005~~) on hillslopes,~~), proclaiming that physical and therefore hydraulic roughness adapts ~~so~~such that flow velocity is a unique function of the overland flow rate independent of slope. ~~All in all, these studies are a~~

1.2 Objectives and hypotheses

In the light of this concise selection of ~~principles and hypotheses which have been published in the past about the organization of~~ studies, we propose that an energy centred perspective on overland flow on hillslopes ~~and river systems but reflect~~might be helpful to better understand the ~~overall notion that~~ co-evolution of hillslope form and functioning and whether those (and other) hydrological systems evolve towards a meta-stable, energetically optimal configuration (Zehe et al., 2013; Kleidon et al., 2014, Bejan and Lorente, 2010). Following the work of Kleidon (2016), we develop the general thermodynamic framework and explain how surface runoff along rivers and hillslopes fit into this setting (sect. 2). We argue that despite the similarity of hillslope surface runoff and river runoff, morphological adaptations and the related degree of freedom of both systems, manifest at distinctly different scales. Mature river elements are mainly fed by the upstream discharge and local base flow, while hillslope elements receive substantial water masses during runoff events through local rainfall and upslope runon. This causes an interesting trade-off along the overland flow path, where mass grows downslope due to flow accumulation, while geopotential height declines. We hypothesize that these antagonistic effects lead to a peak in potential energy of overland flow at a distinct point on the hillslope. This implies an upslope area, where the potential energy of overland flow is growing due to flow accumulation (though water is flowing downslope) before it starts declining in downslope direction. From a thermodynamic perspective, the ability of surface runoff to perform work increases up to the point of maximum potential energy and is then depleted through a cascade of energy conversion processes. Our second hypothesis is thus, that this build-up of potential energy occurs under laminar flow conditions with a low degree of freedom for morphological changes, while the location of potential energy maximum coincides with the emergence of turbulent flow, and with a maximum degree of freedom for morphological changes, including the emergence of rills.

~~Recently, Kleidon (2016) presented a framework which can be applied to each of these principles and beyond. In essence, the mentioned studies investigated different aspects of energy depletion provided by nature, suggesting that energy and energetic~~

flow is organized in time and space. On different scales different mechanisms are involved to a higher or lesser extent but the applicability of thermodynamic laws does not change. Budgeting of energy conversion not only allows the incorporation of all types of free energy but might also help explain why some conversion processes prevail at certain scales. Therefore, our goal is twofold. First, we present the general thermodynamic framework and how surface runoff in river systems and on hillslopes fit into this setting. We propose that despite the similarity of hillslope and river runoff, their energetic functioning is distinctly different. This is because river elements are mainly fed from the upstream discharge (Kleidon et al., 2013) while hillslope elements receive substantial water masses through rainfall input and upslope runon. We will show that the latter causes a trade-off in the potential energy of overland flow as an increasing mass of water flows along a continuously declining geopotential. We hypothesize that these antagonistic effects imply a distinct point in space with maximum potential energy of overland flow. This local maximum is a hot spot as it separates upslope area where the flow gains potential energy from a downslope part, where the hillslope behaves energetically like a river with declining potential energy. This relates to our second hypothesis, that the build-up of energy happens under laminar flow conditions with less dissipation per unit flow rate, whereas more dissipative, turbulent flow should dominate if total potential energy is declining. For steady state energy conversion processes, production of entropy is represented by the distribution of energy gradients in space, and any system would have to optimize these gradients to behave in accordance with any of the mentioned optimization principles. Here we suggest that this optimization happens at several scales and therefore involves different dominant flow processes.

The first application of our thermodynamic framework, presented in sect. 2, zooms on the principal mechanisms involved in steady state energy distribution and therefore gradients of surface runoff on hillslopesframework tests hypothesis 1, by exploring macro scale topographic controls. We explore how different distributions of geopotential along the flow line (cf. Rieke-Zapp and Nearing, 2000)how typical shapes of hillslope topography in combination with different hillslope width functions control flow accumulation and thus overland flow energy in space (sect. the spatial patterns of potential and kinetic energy of surface runoff and energy dissipation along the flow path3). In the second part of the study (sect. 4), we apply our framework to observations of overland flow distinguishing rill- and sheet flow obtained during steady states (sect. 3). rainfall-runoff As these shapes represent different morphological hillslope stages (Kirkby, 1971), shaped by erosive forces of previous surface runoff events (Rieke-Zapp and Nearing, 2005), we expect differences in the energy balance, including the location of the potential energy maximum. The second application of our framework tests hypothesis 2 (sect 4), by analysing the energy balance of surface runoff observed during hillslope scale rainfall simulation experiments in the Weiherbach catchment (Scherer et al., 2012). For this we develop a rill domain for the numerical model Catflow (Zehe et al., 2001), simulate distinctly differentThe experiments and analyse them in terms of overland flow energy and the transition from laminar to turbulent flow. The separationprovide measurements of eroded sediments and total runoff including sheet and rill flow velocities at the lower end of the irrigated stripes, and therefore present an opportunity to explore how rills and rill networks affect the energy balance of surface runoff into . For that purpose, we calibrated an extended version of the Catflow model (Zehe et al. 2001), which accounts for the transition from sheet- and to rill flow allows us, to explorethese experiments, and analysed the effectspatial patterns of runoff accumulation in rills on energetics of overland flow and test our second hypothesis that thepotential energy maximum coincides, kinetic energy and dissipation with respect to the transition from laminar to turbulent flow regimebased on simulated flow depths and velocities.

2 Theory

2.1 Free energy balance of hillslopes as open thermodynamic rainfall-runoff systems

To frame surface runoff processes into a thermodynamic perspective we define the surface of a hillslope as an open thermodynamic system (OTS; Kleidon, 2016). In this sense, the hillslope exchanges mass, momentum, energy and entropy

with its environment (Fig. 1). Rainfall adds mass at a certain height and thus free energy in the form of potential energy along the upper system boundary. Mass and free energy leave the system at the lower boundary due to surface runoff or via infiltration as subsurface flow (Zehe et al., 2013). ~~We~~To express energy conservation of surface runoff, we start very generally with the first law of thermodynamics~~, to express energy conservation of surface runoff~~ in the following form:

$$\frac{dU}{dt} = \frac{d(H)}{dt} + \frac{dW}{dt} \quad (1)$$

Eq. ~~which~~(1) states that a change in the internal energy U [Joule] of a system consists of ~~the transfer of~~ change in heat H ~~[Joule] to the system~~in joule plus the amount of work W ~~[Joule]~~in joule performed by the system. Here, ~~we add~~the performed work ~~to~~dW remains part of the internal energy, as in an open environmental system ~~the amount of energy dW~~ work is usually performed in the system and does not leave ~~the system but rather is converted into some other kind of energy that stays inside the system~~it as it is the case for heat engines (Kleidon, 2016). Note that the capacity of a system to perform work is equivalent to the term "free energy"~~, whereas~~". Solving Eq. (1) for the change in free energy/work reveals hence that a change in heat is associated with ~~the dissipation~~a dissipative loss of free energy and production of thermal entropy. The latter reflects the second law of thermodynamics, which states that entropy is produced during irreversible processes. The free energy of surface runoff at any point on the hillslope corresponds to the sum of its potential and kinetic energy if we neglect pressure work (i.e., assuming constant pressure~~), mechanical work (i.e., no shaft work such as pumps and turbines) and chemical energy. We apply~~) and mechanical work (i.e., no shaft work such as pumps and turbines). ~~Eq. (1) for each energy form, meaning that the difference between in- and outflux of energy causes a gradient, that can be depleted by conversion of energy into another form. For potential energy we consider the part which corresponds to the topographic difference between precipitation input and runoff output as available potential energy, which is fed by an influx of free energy from precipitation and upslope runon. Potential energy of infiltration excess water at the hillslope surface is converted into kinetic energy of overland flow, and kinetic energy is dissipated into heat (Fig. 1). In this two-box scheme we consider only the energies of fluid flow and neglect energy transfer from and to sediment particles.~~

~~To explore the spatial distribution of~~

We apply Eq. (1) to balance both potential and kinetic energy ~~we~~ of surface runoff separately and subdivide the hillslope ~~surface~~ into lateral segments along the horizontal flow path x (Fig. ~~2~~)1), with a given width ~~B~~b and express energy fluxes in ~~W~~watt m^{-1}. Note that differences between in- and outflux of free energy in a hillslope element imply that these are either converted into another form of free energy or are dissipated. The potential energy balance of surface runoff depends on the topographical/ geopotential elevation of the hillslope element, on the corresponding mass inputs due to rainfall and upslope runon, on the mass losses due to infiltration and downslope runoff and on the energy conversion into kinetic energy (Eq. (2)). In our notion potential energy of infiltration excess surface runoff is converted into kinetic energy of overland flow, while kinetic energy is partly dissipated via friction into heat (Eq. (3)), and another part is transferred into erosion and sediment transport. Note that in our two-box scheme (Fig. 1) we consider total energies of fluid flow (mean velocity, though possibly turbulent) and the kinetic energy balance residual D_f does not separate energy transfer to sediments from frictional dissipation.

We can thus write the potential and kinetic energy balance equations for any segment of the hillslope~~:~~ in watt per meter (Table):

$$\frac{dE_f^{pe}(x)}{dt} = J_{f,in}^{pe}(x) - J_{f,out}^{pe}(x) + J_{P,in}^{pe}(x) - J_{Inf,out}^{pe}(x) - P_f(x) = J_{f,net}^{pe}(x) + J_{Peff,net}^{pe}(x) - P_f(x) \quad (2)$$

$$\frac{dE_f^{ke}(x)}{dt} = P_f(x) - D_f(x) + J_{f,in}^{ke}(x) - J_{f,out}^{ke}(x) = P_f(x) - D_f(x) + J_{net}^{ke}(x) \quad (3)$$

Formatted: Font: Italic

Formatted: Font: Italic

Fluxes with superscript "*pe/ke*" relate to potential energy and kinetic energy, respectively. The subscript "*f*" relates to surface runon and runoff, subscript "*inf*" to infiltration and subscript "*P*" to precipitation (see table ~~1). Eq. (~~2) ~~balances~~). Equations (2) and (3) balance changes of potential energy of runoff E_f^{pe} ~~, while Eq. (3) is the~~ and it's kinetic energy ~~balance of surface water~~ E_f^{ke} ~~. We further define~~, also expressed in terms of the net energy fluxes across the segment boundary $J_{f,net}^{pe}, J_{f,net}^{ke}, J_{Peff}^{pe}$; ~~as the net energy fluxes across the systems boundary. All energy fluxes are in watt per meter (Table 1), and the subscript "net" represents the difference of the respective "in" and the "out" fluxes.~~ P_f is the transfer from potential to kinetic energy and D_f ~~is the remaining energy flux, which has not been conserved as potential or kinetic energy of the water flow and leaves the system. D_f is more than~~summarizes the frictional dissipation ~~by friction, as it includes e.g.,~~rate and the work needed for sediment detachment and transport as well as energy that is used to generate turbulent kinetic energy. While dissipation means free energy is lost as heat, kinetic energy transfer to the sediment is not dissipated, as it creates macroscopic motion. ~~In the following, we neglect the kinetic energy transfer to sediments (and other mass) and refer to D_f simply as the dissipation for of potential energy. As generally accepted, we assume that infiltration and precipitation act mostly on the potential energy and neglect their influences on kinetic energy.~~ Along similar lines, one could separate turbulent kinetic energy from kinetic energy of the mean flow when including turbulent velocity fluctuations. By combining Eq. (2) and (3) the total free energy balance of a hillslope segment becomes:

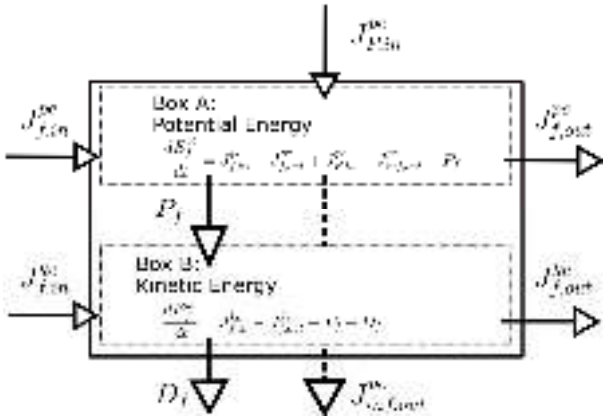

~~**Figure 1: The hillslope surface runoff as a two box open thermodynamic system**~~

~~Combining Eq. (2) and (3) and accounting time dimensionality, the total free energy balance is:~~

$$\frac{dE_f^{pe}(x,t)}{dt} + \frac{dE_f^{ke}(x,t)}{dt} = J_{f,net}^{pe}(x,t) + J_{f,net}^{ke}(x,t) + J_{Peff,net}^{pe}(x,t) - D_f(x,t) \qquad (4)$$

The change in total free energy of ~~the~~ overland flow ~~system~~in a segment is equal to the sum of ~~the differences in the~~ net ~~boundary~~ energy fluxes minus dissipation. In the case of steady state $\left(\frac{dE_f^{pe}(x,t)}{dt} = \frac{dE_f^{ke}(x,t)}{dt} = 0\right)$, the dissipation term D_f can be ~~maintained if the net boundary fluxes are non-zero. It should be noted that within the~~ determined as residual of the steady state energy balance ~~of total free energy the net boundary fluxes of a kind may become negative, therefore seemingly the system exports more energy than is imported. Downslope water movement does not just imply a reduction in its geopotential, but also that additional rainfall mass is added~~. Before we further elaborate on this in section 2.3, we reflect on the relation between the energy balance residual, frictional dissipation, and the related flow laws.

Formatted: Font: Italic
Formatted: Font: Italic
Formatted: Font: Italic
Formatted: Font: Italic

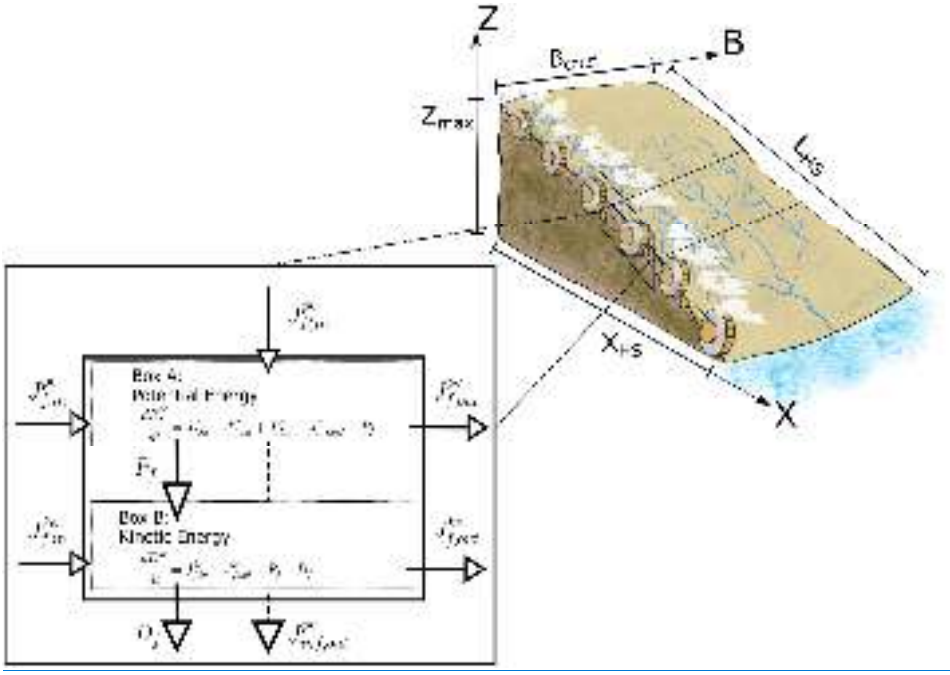

Figure 1: Hillslope open thermodynamic system with spatial division into sub-OTS as a two box open thermodynamic system. Each control volume (sub-OTS) is represented by a prony brake (cf. Leopold and Langbein, 1962)
~~its way. In such a distributed mass accumulating system, it is therefore possible that the gain in mass per unit length adds more~~

2.2 The energy balance residual D_f and frictional dissipation at the hillslope scale

Here, we focus on conversion of potential energy ~~than is converted~~ into kinetic energy~~. From a momentum balance point~~, because the former controls the hierarchy of ~~view this corresponds to an increase in momentum while~~ possible energy conversion in surface runoff. We neglect the subsequent kinetic energy transfer to sediments and turbulent velocity ~~is constant (Kleidon et al., 2013).~~ fluctuations and refer to D_f simply as the dissipation of kinetic energy. The concept could be extended to account for phase transitions from laminar to turbulent flow as well as for kinetic energy transfer to eroded sediment particles. In these cases, D_f needs to be separated into the energy fluxes that a) convert kinetic energy of mean flow into turbulent kinetic structures, b) transfer energy to sediment motion and c) frictional dissipation, while at the same time one needs to include the energy balance of eroded sediments.

Formatted: Highlight

For laminar flow the downslope accumulation of runoff leads to a steeper vertical velocity gradient, which might surpass a critical threshold Reynolds number to create turbulent flow structures (expressed as the relation of inertia to viscous forces). These convert kinetic energy of the mean flow into kinetic energy of small-scale velocity fluctuations, and thereby reduce the kinetic energy and thus velocity of the mean flow. Turbulence in turn provides the power and force to detach and lift sediment particles, which also need to be accelerated (in the simplest case) to the mean flow velocity. Both erosion processes feed again on the kinetic energy of the mean flow, while particle detachment feeds also on kinetic energy of rain drops. In the light of these thoughts, one can expect D_f to be larger for turbulent than for laminar flow, when using the mean flow velocities to calculate E_f^{ke}, and D_f should also be larger in the case of erosion and sediment transport. Both processes extract kinetic energy and consequently reduce mean flow velocities, as corroborated by Ali et al. (2012) for energy transfer to sediments in experiments of runoff on erodible beds. This energy transfer has implications for the inverse estimate of roughness coefficients

from rainfall simulation experiments (also for those we use in section 4). The important point to stress here, is that in general an increase of an observed (apparent) resistance to flow due to a reduced mean flow velocity can but must not necessarily imply that a larger frictional dissipation is the underlying cause.

Govers et al. (2000) summarize the methods, which are still in use today for estimating how frictional dissipation controls steady state runoff velocities as a function of roughness, essentially representing the degree of free energy loss from the mean flow. Most approaches focus on the generalization of a friction coefficient in time and/or space for a given surface area where runoff occurs, which is expressed by a general friction law that relates unit width discharge q to flow depth d and topographic slope S:

~~symbol~~ $q = c_1 d^{c_2} \sqrt{S}$ ~~unit~~ (5)

~~**Table 1: Overview of the different symbols used in this study**~~

~~description~~		
~~U~~	~~[kg m^{2}s^{-2}]~~	~~**internal energy of a thermodynamic system**~~
~~W~~	~~[kg m^{2}s^{-2}]~~	~~available energy to perform work by the thermodynamic system~~
~~H~~	~~[kg m^{2}s^{-2}]~~	~~thermal energy of the thermodynamic system~~
~~$E_f^{pe/ke}$~~	~~[kg m$\cdot$s^{-2}]~~	~~Potential- or kinetic energy of the water flow~~
~~$J_{f,in/out}^{pe/ke}$~~	~~[kg m$\cdot$s^{-3}]~~	~~Potential- or kinetic energy flux entering or leaving the system~~
~~$J_{P,in}^{pe}$~~	~~[kg m$\cdot$s^{-3}]~~	~~precipitation entering the system as potential energy flux~~
~~$J_{inf,out}^{pe}$~~	~~[kg m$\cdot$s^{-3}]~~	~~infiltration leaving the system as potential energy flux~~
~~P_f~~	~~[kg m$\cdot$s^{-3}]~~	~~power to create kinetic energy of system~~
~~D_f~~	~~[kg m$\cdot$s^{-3}]~~	~~dissipation of free energy of flow into different kind of energy~~
~~v~~	~~[m$\cdot$s^{-1}]~~	~~velocity of runoff, parallel to bed slope~~
~~v_z~~	~~[m$\cdot$s^{-1}]~~	~~vertical fraction of v~~
~~ρ~~	~~[kg m^{-3}]~~	~~density of water with value of 1000~~
~~g~~	~~[m$\cdot$s^{-2}]~~	~~gravitational acceleration with value of 9.81~~
~~Q~~	~~[m^{2}s^{-1}]~~	~~discharge~~
~~h~~	~~[m]~~	~~water height above hillslope end (h=z+d)~~
~~B~~	~~[m]~~	~~hillslope width~~
~~P_{eff}~~	~~[m$\cdot$s^{-1}]~~	~~effective rainfall intensity~~
~~d~~	~~[m]~~	~~water column depth of surface runoff~~
~~n~~	~~[m$^{-1/3}$.s]~~	~~manning coefficient~~
~~S~~	~~[-]~~	~~slope of bed level~~
~~z~~	~~[m^2.s^2]~~	~~geopotential of bed level to reference level~~
~~X~~	~~[m]~~	~~length of hillslope, parallel to reference surface~~
~~L~~	~~[m]~~	~~length of hillslope, parallel to bed level~~
~~R~~	~~[m]~~	~~hydraulic radius~~
~~A~~	~~[m^2]~~	~~wetted area of discharge~~
~~r~~	~~[m]~~	~~radius of semi-circled rills~~
~~m~~	~~[-]~~	~~number of semi-circled rills~~
~~τ_b~~	~~[kg m^{-1}s^{-2}]~~	~~bed shear stress~~
~~c_{FC}~~	~~[-]~~	~~Flow accumulation coefficient of CATFLOW-RILL model~~
~~α,β,γ~~	~~[radians]~~	~~Angles of CATFLOW-RILL hillslope surface~~
~~Re~~	~~[-]~~	~~Reynolds number of surface runoff~~
~~f_{crit}~~	~~[kg m^{-1}s^{-2}]~~	~~Critical erosion force of surface runoff~~

Formatted: Justified, Indent: Left: 0,09 cm
Formatted Table
Formatted: Font: 11 pt, English (United States)
Deleted Cells
Formatted: Centered
Formatted: Font: 11 pt, English (United Kingdom)

~~2.2 The hillslope surface as open thermodynamic system~~

~~To frame surface runoff processes into a thermodynamic perspective we define the surface of a hillslope as an open thermodynamic system (OTS; Kleidon, 2016). In this sense, the hillslope exchanges mass, momentum, energy and entropy~~

with its environment (Fig. 1 and 2). Rainfall adds mass at a certain height and thus free energy in the form of potential energy along the upper system boundary. Mass and free energy leave the system at the lower boundary due to surface runoff or via infiltration as subsurface flow (Zehe et al., 2013). In order to analyse the distribution of energy conversion processes in space we distinguish open thermodynamic subsystems (OTS_{sub}) that are assumed to be in steady state as shown in Fig. 2.

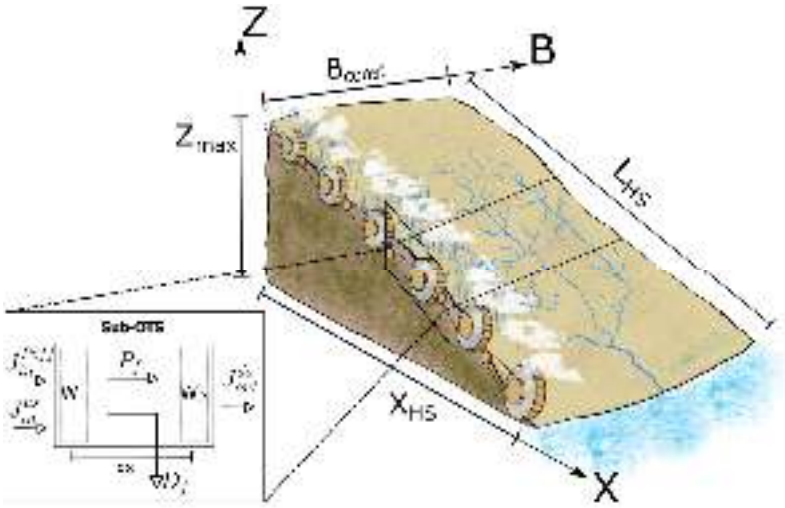

Figure 2: Hillslope open thermodynamic system with spatial division into sub-OTS and energy flows from upstream and downstream ($J_{in}^{us} = J_{f,in}^{pe} + J_{f,in}^{ke}$ *and* $J_{out}^{ds} = J_{f,out}^{pe} + J_{f,out}^{ke}$) as well as free energy reservoirs W_1 and W_2. Each control volume (sub-OTS) is represented by a pony brake (cf. Leopold and Langbein, 1962)

For each OTS_{sub} we apply Eq. (4) in steady state and express potential and kinetic energy of the fluxes through hydraulic variables (see Appendix A for derivation) to obtain:

$$D_f(x) = J_{f,net}^{pe}(x) + J_{Peff,net}^{pe}(x) + J_{f,net}^{ke}(x)$$

$$= \rho * g * \left(-\frac{dQ(x)}{dx} * h(x) - \frac{dh(x)}{dx} * Q(x) + P_{eff}(x) * h(x) * B(x) \right) \quad (5)$$

$$-\frac{1}{2} * \rho * \left(\frac{dQ(x)}{dx} * v(x)^2 + 2 * v(x) * \frac{dv(x)}{dx} * Q(x) \right)$$

Where Q [$m^3 s^{-1}$] is the overland flow rate, v [$m\ s^{-1}$] the average flow velocity, h [m] the water height above the hillslope outlet, ρ [$kg\ m^{-3}$] the density of water, g [$m\ s^{-2}$] gravitational acceleration and P_{eff} [$m\ s^{-1}$] the difference between rainfall intensity and infiltration. The energy, which is dissipated per unit length depends on the net potential plus the net kinetic energy flow plus the additional energy input per time through precipitation. With the assumption that change of velocity in space is close to zero ($v=v_{const}$) and $\frac{dQ(x)}{dx} = P_{eff} * B(x)$ Eq. (5) becomes:

$$D_f(x) = -P_{eff} * \rho * g * B(x) * \frac{v_{const}^2}{2 * g} - Q(x) * \rho * g * \frac{dh(x)}{dx} \quad (5\ a)$$

For c_1 and c_2 Eq. 5a, we can see that the first term scales with P_{eff} and the second with Q. With precipitation usually decreasing and discharge increasing in downstream direction, there will be a flow path length where we can reduce Eq. (5 a) to its second term:

~~$$D_f(x) = -Q(x) * \rho * g * \frac{dh(x)}{dx}$$~~ ~~(5 b)~~

~~This could be the case for a larger stream and explain how systems with small variation of mass minimize energy dissipation by flattening of their geopotential gradients ($\frac{dh(x)}{dx}$ approaches very small values). As more and more mass accumulates along the flow path, dissipation of discharge power is less controlled by changes in velocity or mass. This results in an increasingly flattened geopotential gradient and therefore a negative exponential distribution of geopotential (Leopold and Langbein, 1962). In the literature Eq. (5b) is also called stream power (Bagnold, 1966) and is used to calculate the force τ [N m^{-2}] that acts on bed material per unit area ("shear stress", with d [m], as depth of water column):~~

~~$$\tau(x) = \frac{D_f(x)}{v(x) * b(x)} = -d(x) * \rho * g * \frac{dh(x)}{dx}$$~~ ~~(6)~~

~~2.3 Steady state spatially distributed energy of overland flow: Rivers vs. hillslopes~~

~~The steady state distribution of energy and its gradients within a system stands in feedback with the flow and flow accumulation. The larger the gradient, the higher the flow, which leads to a faster depletion of the gradient and less flow. In hydraulic sciences the geopotential gradient of a runoff system is usually approximated with the slope S [m m^{-1}] of the riverbed (Bagnold, 1966), reducing Eq. (6) to the depth slope product and facilitating the calculation of depth averaged momentum balances by use of a general friction law:~~

~~$$Q = c_1 * b * d^{c_2} * \sqrt{S}$$~~ ~~(7)~~

~~Where c1 and c2~~ are coefficients, which vary for Manning-Strickler (Manning's n ~~[s m$^{-1/3}$]~~), Chezy (C ~~[m$^{1/2}$ s^{-1}]~~) and Darcy-Weißbach (f ~~[-]~~) (Singh et al., 2003, table 1).

Table ~~2:~~1: Coefficients of general friction law

	c_1	c_2
Manning-Strickler	$\frac{1}{n}$	$\frac{5}{3}$
Chezy	C	$\frac{3}{2}$
Darcy-Weißbach	$2 * \left(\frac{2g}{f}\right)^{0.5}$	$\frac{3}{2}$

Although it is known that friction coefficients on hillslopes vary with the degree of roughness element inundation (Lawrence, 1997), as well as sediment transport concentrations and are transient (Abrahams et al., 1994), mean flow velocities are in practice estimated by using constant values. Without additional information about the flow regime and transport process, these coefficients provide, as explained above, an uncertain estimate of frictional energy dissipation of free energy into heat and related entropy production (Govers et al., 2000). Furthermore, experiments by Govers (1992) for rill flow as well as by Nearing et al. (2017) for sheet flow indicate that friction coefficients vary across the hillslope during steady state. They even seem to be spatially organized, as these studies found that mean runoff velocity can be solely estimated by the runoff rate, independent of topographic slope or rainfall intensities. For the analysis presented in sect. 3, we use one of these empirical formulae which was developed by Nearing et al. (2017) for surface runoff on stony hillslopes:

$$v = 26.39 * q^{0.696} \quad (6)$$

Eq. (6) implicitly incorporates variable friction coefficients, as flow velocity v is a unique function of unit width discharge q. The advantage of Eq. (6) is that we can back-calculate the spatial distribution of potential energy without estimating frictional dissipation as a lumped constant, such as it is the case in Eq. (5). Obviously, this formula might not be applicable to hillslopes

Formatted: Font: Italic

Formatted: Font: Italic

Formatted: Font: Italic

with different soil properties and vegetation, but thoughtful design of future experiments might reveal that the hypothesized independence of flow velocity is generalizable.

For the analysis of the rainfall simulation experiments in section 4, the derivation of a similar empirical formula is beyond the data this study has at hand. This implies that absolute values of frictional dissipation rates presented section 4 are uncertain. But they are nevertheless a useful starting point, as our focus lies on their spatial patterns and the relative differences depend on macroscale properties (measured velocities and runoff rates of rill and sheet flow in this case), which are well captured by these experiments. So even without explicit inclusion of the energy transfers between mean flow and turbulent structures or sediment particles, the analysis of the spatial distribution of potential energy is helpful to understand constraints of runoff and morphological process as well as the sensitivity to different hillslope forms or the presence of rill networks

Table 2: Overview of the different symbols used in this study

Symbol	Unit	Description
U	kg m^2 s^{-2}	internal energy of a thermodynamic system
W	kg m^2 s^{-2}	available energy to perform work by the thermodynamic system
H	kg m^2 s^{-2}	thermal energy of the thermodynamic system
$E_f^{pe/ke}$	kg m s^{-2}	Potential- or kinetic energy of the water flow
$J_{f,in/out}^{pe/ke}$	kg m s^{-3}	Potential- or kinetic energy flux entering or leaving the system
$J_{P,in}^{pe}$	kg m s^{-3}	precipitation entering the system as potential energy flux
$J_{inf,out}^{pe}$	kg m s^{-3}	infiltration leaving the system as potential energy flux
P_f	kg m s^{-3}	power to create kinetic energy of system
D_f	kg m s^{-3}	dissipation of free energy of flow into different kind of energy
v	m s^{-1}	velocity of runoff, parallel to bed slope
ρ	kg m^{-3}	density of water with value of 1000
g	m s^{-2}	gravitational acceleration with value of 9.81
ν	m^2 s^{-1}	Kinematic viscosity with value of 10^{-6}
Q	m^3 s^{-1}	discharge
h	m	water height above channel bank (h=z+d)
b	m	hillslope width
b_r	m	Bottom width of trapezoidal rill cross-section
q	m^2 s^{-1}	Unit width discharge
I	mm h^{-1}	rainfall infiltration excess intensity
d	m	water column depth of surface runoff
n	m$^{-1/3}$ s	Manning coefficient
C	m s$^{-1/3}$	Chezy coefficient
f	-	Darcy-Weißbach coefficient
S	-	topographic slope
z	m	geopotential of bed level to reference level
X_{HS}	m	length of hillslope, parallel to reference surface
L_{HS}	m	length of hillslope, parallel to bed level
R	m	hydraulic radius
A	m^2	wetted area of discharge
τ	kg m^{-1} s^{-2}	bed shear stress
C_f	-	Flow accumulation coefficient of Catflow model
α, β, γ	radians	Angles of Catflow hillslope surface
Re	-	Reynolds number of surface runoff
Re_c	-	Critical Reynolds number of surface runoff

k	-	Relative roughness
Q_{sed}	kg s^{-1}	Sediment discharge
C_{sed}	kg m^{-3}	Sediment concentration
d_{50}	µm	Mean sediment particle diameter

2.3 The steady state energy distribution of surface runoff and transitions between flow regimes

We come back to the steady state free energy balance of surface runoff (Eq. (4)), which allows an estimation of the term D_f as energy balance residual. For convenience, we express the energy fluxes on the right-hand side by the hydrological variables overland flow rate Q in m^3 s^{-1}, mean flow velocity v in m s^{-1}, infiltration excess intensity I in mm h^{-1} (difference between rainfall intensity and infiltration rate), and water height above the channel bank h in m (see Appendix A for derivation):

$$\begin{aligned} D_f(x) &= J^{pe}_{f,net}(x) + J^{pe}_{Peff,net}(x) + J^{ke}_{f,net}(x) \\ &= \rho g\left(-\frac{dQ(x)}{dx}h(x) - \frac{dh(x)}{dx}Q(x) + I(x)h(x)b(x)/(3.6\times 10^6)\right) \\ &\quad -\frac{1}{2}\rho\left(\frac{dQ(x)}{dx}v(x)^2 + 2v(x)\frac{dv(x)}{dx}Q(x)\right) \end{aligned} \quad (7)$$

Where ρ (kg m^{-3}) is the density of water, and g (m s^{-2}) is gravitational acceleration.

The terms in the first bracket reveal the antagonistic effects of a downslope growing discharge due to flow accumulation and the decline in topographic elevation on potential energy. As stated in our first hypothesis, we expect that this trade-off leads to a local potential energy maximum. While the existence of such a maximum can in fact already be confirmed by a re-analysis of the experiments of Emmet (1970) (Fig. 2, sect. 3.), the existence of such a maximum is usually not discussed in the case of stream flow. This is because Eq. (7) simplifies in streams to Eq. (8), as kinetic energy fluxes are much smaller than potential energy fluxes and with increasing discharge the mass balance gets more and more dominated by upstream runon while precipitation input becomes marginal:

$$D_f(x) = -Q(x)\rho g\frac{dh(x)}{dx} \quad (8)$$

In the literature Eq. (~~To highlight the difference between rivers and hillslopes Fig. 3 compares the spatial distributions of potential energy along a flow path in a river system and on a hillslope. We take the Rhine from Basel to its mouth at Emmerich as an example, and we calculated potential energy E_{pot} [kg m^2 s^{-2}] and volumetric potential energy E^{SP}_{pot} [kg m^{-1} s^{-2}] ($E^{SP}_{pot} = E_{pot}/Q$) from the mean yearly discharge and the water depth above sea level (data obtained from LUBW, 2021). Furthermore, we digitized the results of Emmett (1970) from his experiments on hillslope plots and computed E_{pot} and E^{SP}_{pot} from measured water depth above outlet reference level and mean flow velocity.~~

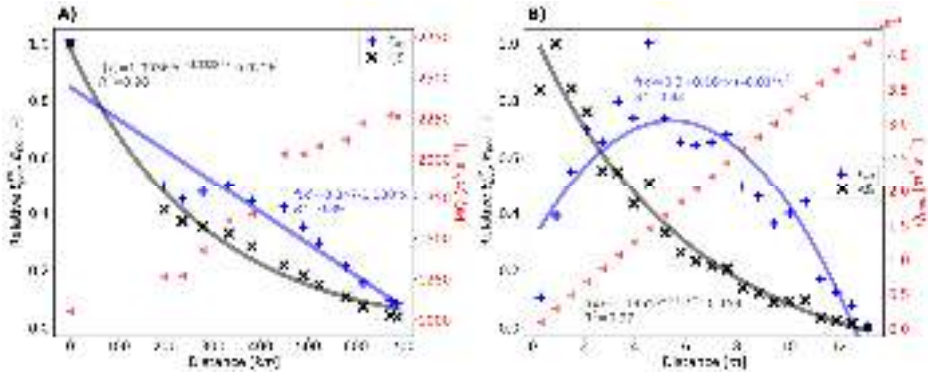

Figure 3: a) Relative volumetric-, total potential energy and average annual discharge MQ along the River Rhine; b) Relative volumetric-, total potential energy and accumulated discharge Q_{cum} on hillslope plot (experiment "New Fork River Site 1", Emmett (1970))

From the plots in Fig. 3, we can see that in river and hillslope systems alike, volumetric energy E_{pot}^{SP} as well as its gradient minimize along the flow path. Or differently stated, the energy expenditure per unit discharge minimizes in downstream direction (solid black lines). This is very much in line with the principle of Rodriguez Iturbe et al. (1992) and Yang (1976). Interestingly however, the distribution of total potential energy along flow path is different for hillslope and river systems. The river Rhine distributes the loss of potential energy equally along its flow path and thus performs work uniformly on its course, as stated in the second principle of Rodriguez Iturbe et al. (1992). The distribution of total energy on hillslopes follows a quadratic function, which rises to a maximum at 6 m and declines further downslope. This finding is on the one hand straightforward, because if mass is accumulatively added along the flow path, whilst loosing geopotential, there must be a maximum somewhere downslope. On the other hand, we think this finding is astonishing as a positive energy gradient in downslope direction poses somewhat of a challenge to our common friction laws. In section 3 we explore how this maximum in potential energy depends on rainfall intensity and hillslope form.

We have already pointed out, that surface runoff on hillslopes has a transitional character. As also measured by Emmett (1970), the flow regime upslope of the hillslope starts laminar, transitioning to mixed and finally turbulent flow further downslope. Upslope, very shallow water depths limit erosion to the impact by raindrops, so called splash erosion and soil creep, which is erosion through gravity, while further downstream erosion by turbulent drag of the water flow is dominant (Shih and Yang, 2009). Similarly, there exists a minimum flow path length for surface runoff to occur, sometimes at the beginning referred to thread flow, which transitions into shallow sheet flow (Dunne and Dietrich, 1980) and on bare soils even farther downslope forms rill flow. This transitional character of runoff on hillslopes is represented in Fig. 4.

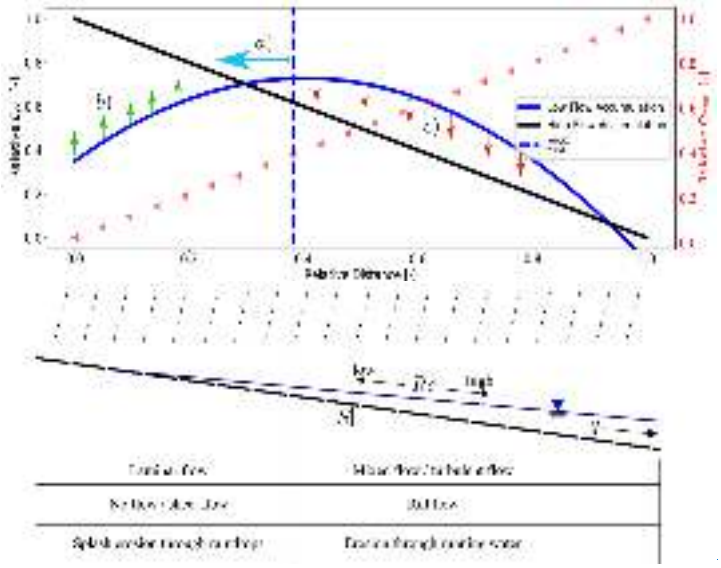

Figure 4: Simplification of overland flow 8) is also called stream power (Bagnold, 1966) and is used to calculate the force τ in N m^{-2} that acts on bed material per unit area ("shear stress", with d in m, as depth of water column) for river discharge:

$$\tau(x) = \frac{D_f(x)}{v(x) * b(x)} = -d(x)\rho g \frac{dh(x)}{dx} \quad (9)$$

Mostly dh/dx is approximated by topographic slope, leading on hillslopes to an underestimation of the driving water level gradient in flat terrain and an over-estimation of the gradient on steep slopes (Govers et al., 2000). This is also related to the experimental findings of Ali et al. (2012), who concluded that sediment transport capacity is weakly correlated to calculated bed stress and attributed this finding to the transfer of energy to the detachment of sediment. It is therefore evident that the approximation of lost energy by topographic slope and fixed roughness parameters alone cannot provide closure for the energy balance of surface runoff, and a closer look at involved energy conversion processes seems necessary. After the upslope onset, surface runoff accumulates as very shallow, laminar sheet flow (Dunne and Dietrich, 1980), which is, according to Eq. (9), yet too small to trigger erosion and perform significant work to the hillslope surface. Resistance to flow at this stage relates to the individual drag force of exposed sediment particles, leading to an increase of roughness for larger flow depths (Lawrence, 1997). As soon as the particles are inundated the kinetic energy of overland flow can be enlarged or even maximized as a further increase of flow depth results in a reduction of local roughness. Here the flow is still laminar, meaning that mean flow velocities and kinetic energies in the mean flow are larger than for turbulent flow. With further increase of flow accumulation and flow depth, the velocity profile in the boundary layer becomes steep enough to create turbulence, so less potential energy is converted into kinetic energy of the mean flow, which lets resistance to the mean flow appear larger. In fact, the reduced kinetic energy of the mean flow is also due to the increase of kinetic energy of turbulent structures, which in turn provide the necessary power to erode the surface and deplete the topographic gradient by redistribution of soil material through rill networks.

Rill structures form on event to seasonal timescales due to a fast positive feedback (Rieke-Zapp and Nearing, 2005). On a longer timescale the redistribution and export of soil material restructures entire topographic hillslope profiles such that typical shapes can be attributed to a dominant erosion process (Kirkby, 1971; Beven, 1997). The latter change in space along the flow path, and therefore in close connection to the flow regimes (Shih and Yang, 2009; cf. Fig. 2). At the upslope divide erosion is mostly influenced by gravity, resulting in soil creep. With flow accumulation in downslope direction, the particles eroded by

raindrop splash can be transported by surface runoff, until surface runoff becomes turbulent and can erode and transport particles as soil wash. The spatial organization of transition processes (also called threshold processes) can be described by the relative contribution of internal and external forces. Turbulence emerges when gravitational (external) force surpasses a certain threshold in relation to viscous (internal) forces. Similarly, soil wash erosion relates to externally induced bed stress by runoff while soil creep depends on internal resistance factors of the soil matrix. We therefore propose, as stated in our second hypothesis, that both process transitions are linked through their external forcing, which is attributed to the energy gradient of surface runoff. The distribution of surface runoff energy and its gradient provide therefore insights on erosional as well as flow regimes.

In the following we apply our framework to test our hypotheses on two related temporal and spatial scales. In section 3, we analyse the distribution of energy at the macroscale, representing the hillslope as an open thermodynamic system which adapts morphologically to the distribution of gradients and fluxes on long timescales. To this end we analyse steady state runoff on typical hillslope profiles that reflect according to Kirkby (1971) dominant erosion processes "soil creep", "rain splash" and "soil wash". In section 4 we analyse the energy balance of surface runoff observed during short term rainfall simulation experiments, where runoff concentrates in rills and distributes energy into a sheet- and a rill domain.

In both sections we explore how the transition of flow regime and erosion processes on hillslopes ~~(modified after Shih and Yang (2009)) as a function of Reynolds number *Re* and distribution of potential energy~~

~~In section 4, we explore whether this transition of flow regimes on hillslopes (from laminar to turbulent or sheet to rill flow) relates to the~~ relate to the distribution of energy and its local maximum. ~~Our rationale is that laminar flow is less dissipative than turbulent flow, and laminar conditions might therefore be related to the build-up of energy (Fig. 4, relative distance 0 until E_{pot}^{MAX}), while the stronger dissipative character of mixed and turbulent flow should be related to a decrease of total energy (Fig. 4, relative distance E_{pot}^{MAX} until 1.0).~~ We want to stress that we speak of laminar flow if there is a clear dependence between flow Reynolds number of surface runoff and friction coefficient (Phelps, 1975). For purpose of comparison with earlier studies of hydraulics of surface runoff (Emmett, 1970; Parsons et al., 1990) we calculate flow Reynolds number *Re* as per Eq. (~~8~~10), relating the characteristic length of ~~Hortonian~~ surface runoff to flow in a fully filled circular pipe. Here, ~~*v*~~*v* represents the depth averaged flow velocity, *R* the hydraulic radius and ν is the kinematic viscosity with a value of 10^{-6} ~~[~~$m^2\ s^{-1}$~~]~~.

$$Re = 4 * \frac{v * R}{\nu} \quad \frac{vR}{\nu} \qquad (8\,10)$$

3~~. A first order assessment of macro-topographic~~ Topographic controls on ~~Hortonian~~the surface runoff ~~and related~~ energy ~~conversions~~ balance terms – a first-order assessment

To clarify and test our hypothesis, we digitized results of rainfall runoff experiments on hillslope plots from Emmett (1970) and plotted potential energy E_f^{pe} and specific potential energy $E_f^{pe,SP}$ ($E_f^{pe,SP} = E_f^{pe}/Q$) (Fig. 2, upper part) in parallel to a sketch of surface runoff on a hillslope and the related flow and erosion process transitions (Fig. 2, lower part). E_f^{pe} and $E_f^{pe,SP}$ were calculated from measured water depth above outlet reference level and mean flow velocity.

The accumulation of mass along a declining geopotential leads to a maximum of potential energy in space, dividing the flow path into a section where energy is gained (Fig. 2, arrow a) and a section where energy is depleted (Fig. 2, arrow b). In between these two sections (Fig. 2, area highlighted in grey), depletion of potential energy is balanced by the energy influxes of runoff accumulation and rainfall. Volumetric energy $E_f^{pe,SP}$ as well as its gradient decrease along the flow path. Or differently stated, the energy expenditure per unit discharge decreases in downstream direction (solid blue line). This is very much in line with the previously mentioned principles of Rodriguez Iturbe et al. (1992) and Yang (1976) of minimum stream power in river streams. To our knowledge a separation of the runoff system into an energy production and energy depletion zone has not been

investigated so far but could have consequences on our understanding on the transitional formation of runoff and erosion processes on hillslopes.

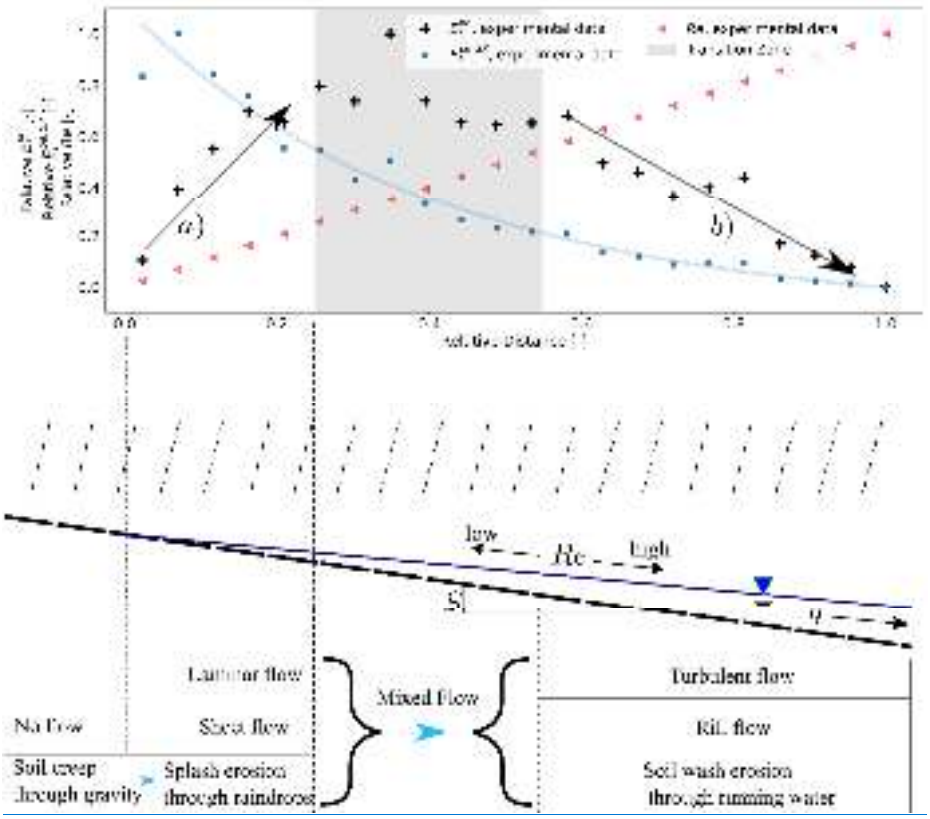

Figure 2: Upper Part: Digitized results from rainfall simulation experiments at New Fork River 1 (Emmett, 1970), expressed as normalized potential energy E_f^{pe}, specific potential energy $E_f^{pe,SP}$, and Reynolds number Re; Lower Part: Simplification of overland flow processes on hillslopes (modified after Shih and Yang (2009)) as a function of Reynolds number *Re* and distribution of potential energy

The transition from a laminar into a turbulent flow regime is indicated by ranges of critical Reynolds-number Re_c, which depend on the type of flow as well as relative friction. While the Re_c of circular pipe flow is roughly 2300 (Schlichting and Gersten, 1955), Emmett (1970) determined in field and laboratory experiments Re_c of sheet flow between 1500 to 6000. Later Phelps (1975) pointed out that for sheet flow over rough surfaces Re_c depends on relative friction k, that is the size of an average sediment particle to the depth of the flow. He showed that for k values of 0.5, Re_c can be as low as 400. For the results presented in Fig. 2, *Re* was calculated with average depths and mean velocities along the slope direction and increased linearly up to 1368 at the lower end of the experimental plot. As however an analysis of the flow patterns suggests, local *Re* at points where flow converges into rills is likely to be much larger. A transition from laminar to turbulent flow regime in rills is therefore likely to correspond in Fig. 2 to a flow path distance within the highlighted transition zone between increase and decrease of potential energy (mixed flow).

3.1 ~~Definition of~~Typical hillslope forms and width functions

In this section, we explore how typical hillslope configurations and effective rainfall forcing, control runoff accumulation and related energy conversions. ~~We distinguish four typical hillslope forms, characterized by either a linear, sinusoidal, exponential or a negative exponential geopotential function along a representative flow path x (Fig. 5a):~~We distinguish three typical hillslope forms, which are related to a dominant erosion process (Kirkby, 1971). Equation (11) defines the distribution of geopotential along a representative flow path. The coefficients m_1 and m_2 describe the relative contributions of accumulated discharge and topographic slope to sediment transport ($Q_{sed} \propto Q^{m_1} S^{m_2}$). According to Kirkby (1971) the region $m_1 < 1$ is therefore related to a hillslope profile that was formed by diffusive erosion processes (soil creep or rain splash), whereas the region $m_1 > 1$ corresponds to more advective erosion processes with higher sediment transport capacities (soil wash, river flow). We can therefore use these empirical coefficients to describe the transition of one regime (diffusive erosion/ transport) into another (advective erosion/ transport), if appropriate boundary conditions (rainfall and infiltration rates, vegetation, etc.) allow for long enough feedback to reach steady state.

$$z_{lin}(x) = -\frac{z_{max}}{x_{HS}} * x + z_{max} \quad Z(x) = Z_{max} * \left(1 - \left(\frac{x}{X_{HS}}\right)^{\frac{1-m_1}{1+m_2}}\right) \qquad (9\text{ a}11)$$

$$z_{sin}(x) = \frac{z_{max}}{2} * \cos\left(\frac{x}{x_{HS}} * \pi\right) + \frac{z_{max}}{2} \qquad (9\text{ b})$$

$$z_{exp}(x) = e^{-x+2+k} * z_{lin}(x) \qquad (9\text{ c})$$

$$z_{neg}(x) = -e^{x+k} * -z_{lin}(x) \qquad (9\text{ d})$$

~~All~~A rough relation between coefficients m_1 and m_2 and corresponding erosion regions is shown in Fig. 3a (after Kirkby, 1990; cited in Beven, 1996). For selection of the coefficients that we use to relate hillslope ~~forms~~form and sediment erosion/ transport regime, we digitized the upper and lower limits and computed a mean curve from which we extracted the coefficients m_1 and m_2 in accordance to ranges indicated by Kirkby (1971). In our example, all hillslopes start at ~~z_{max}~~$Z_{max} = 10$ m, the maximum ~~specific~~ geopotential in ~~$m^2 s^{-2}$~~meter above stream bank, and end at zero~~,~~ at the hillslope end ($X_{HS} = 100$ m, cf. Fig. 3b), depleting all available geopotential gradients~~. In our examples, we assumed z_{max} as the specific geopotential of 10 m altitude multiplied by the gravity of the earth of 9.81 $m^2 s^{-2}$, and a projected hillslope length X_{HS} of 100 m. k is a smoothing factor for the exponential functions and equals 0.01 m^{-1}. These forms have been chosen as they represent~~ on the ~~different geomorphological stages of a~~ hillslope ~~under erosion in time, starting with z_{neg} as the youngest formation (largest gradients towards the end) and ending with z_{exp} and z_{sin} as older formations (smaller gradients towards the end).~~ We then combine these forms with three different width distributions, which are either constant~~,~~ (const), converging (conv) or diverging ~~(Fig. 5a, and b).~~(div) (Fig. 3c). In our analysis we keep the projected area constant at 5000 m^2 for all configurations, which results in an equal total surface runoff from all hillslope forms for a given effective rainfall intensity. Finally, we computed steady state surface runoff for effective rainfall intensities of 5-, 10-, 20- and 50-mm hr^{-1}~~ either without runon (Q_0=0, Fig. 5c) or with 20 kg s^{-1} runon (Q_0=0.02 $m^2 s^{-1}$, Fig. 5d), which is roughly a quarter of the maximum accumulated runoff at 50 mm hr^{-1} rainfall. It should be noted that we considered one case with no rainfall and runon only (I=0; Q_0>0, Fig. 5d). We included this scenario to highlight the differences between runon without rainfall accumulation and runoff with rainfall accumulation when calculating spatial energy dynamics. The differently dotted lines in Fig. 5b, c~~(Fig. 3d). The differently dotted lines in Fig. 3c, and d represent the three hillslope width distributions and show their influence on runoff accumulation. ~~Nevertheless, the total runoff at the end of the hillslope is independent of width distribution as the projected area remains equal for all hillslope forms.~~

Formatted: Centered
Formatted Table
Formatted: Superscript

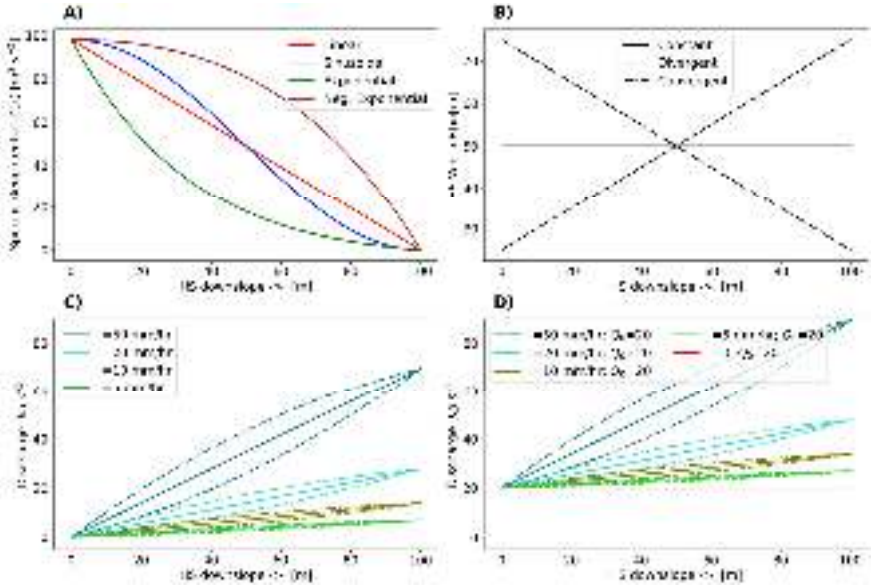

~~Figure 5: Topography and width of the different hillslopes (panels a and b), resulting steady state discharge along the hillslope for the case of no and constant runon of 20 kg s^{-1} (panels c and d). The line types in panels c and d correspond to the width functions in panel b~~

For all combinations of runoff accumulation and hillslope topography, we computed the steady state spatial distribution of water mass and flow velocity using Eq. (~~7) and Manning's n = 0.1 s m$^{-1/3}$~~6). From the ~~spatial~~computed hydraulic variables, we then calculated the distribution of ~~energy, we then computed fluxes of~~ potential ~~flow~~ energy ~~E_f^{pe}~~, flux J_f^{pe} and kinetic ~~flow energy E_f^{ke}, effective rainfall and finally energy expenditure D_f per unit flow length with Eq. (4)~~energy flux J_f^{ke} (see Appendix A ~~for details of computation~~).

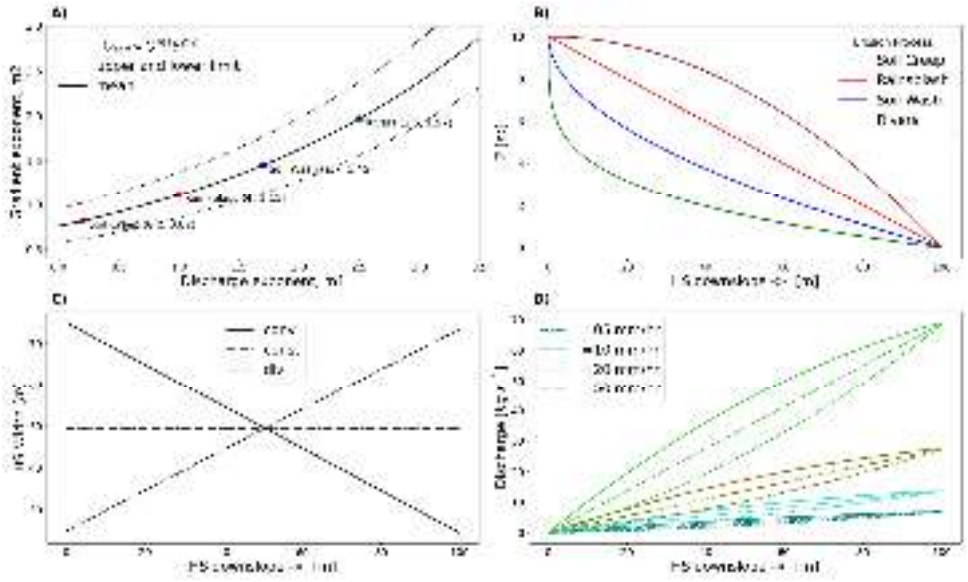

Figure 3: a) Discharge (m_1) and gradient (m_2) exponent (after Kirkby 1990, cited in Beven, 1996) for characterizing sediment transport capacity; b) Typical hillslope (and river) profiles as result of dominant erosion process (Kirkby, 1971); c) Assumed width distributions along flow path; d) Resulting steady state discharge along the hillslope for different rainfall infiltration excess intensities. The line types in panel d correspond to the width functions in panel c.

3.2 Spatial maxima of potential energy

Generally, we found that the trade-off of downslope mass accumulation and declining geopotential leads to a distinct potential energy maximum, which has a clear dependence on the slope form, width function and strength of rainfall forcing ~~(Fig. 6).~~(Fig. 4). This implies that the hillslope can be sub-divided into three classes of spatial energy dynamics:

1) $\frac{dE_f^{pe}(x)}{dx} > 0$
2) $\frac{dE_f^{pe}(x)}{dx} = 0$
3) $\frac{dE_f^{pe}(x)}{dx} < 0$

Within the first interval potential energy flux increases along the flow path, as the additional mass from rainfall adds more energy to the sub-OTS than flows out. At a certain distance (interval 2), energy ~~outflow~~outflux equals energy ~~input~~influx through precipitation plus upstream inflow and we observe an energetic maximum. Within the third interval, energy ~~outflow~~outflux is continuously larger than energy ~~inflow~~influx, effectively depleting the accumulated geopotential of interval 1.

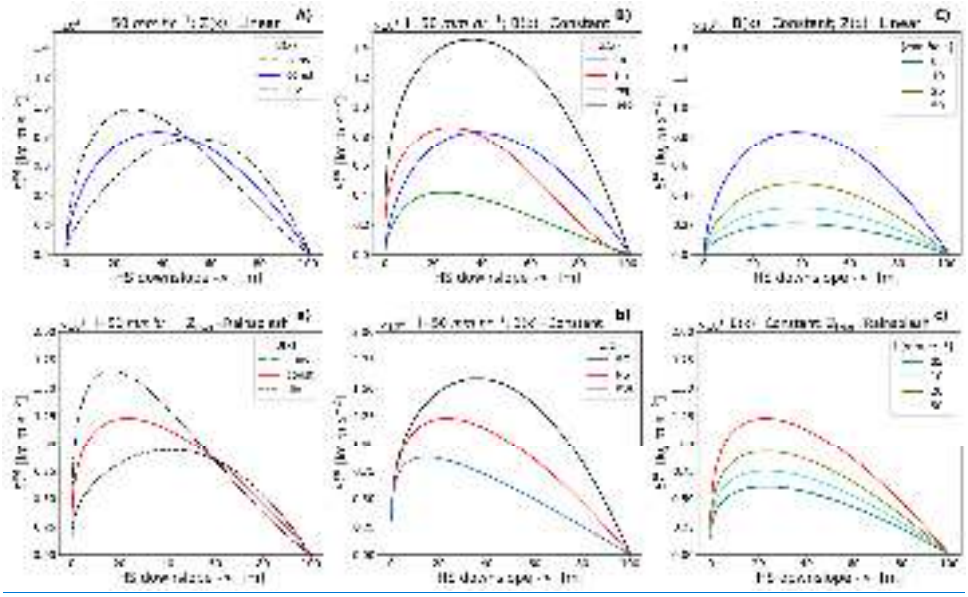

Figure ~~6:~~4: Distribution of potential energy E_f^{pe} per unit length ~~in [~~(Joule m^{-1}~~]~~) as a function of a) hillslope width b) geopotential distribution (form) and c) rainfall intensity I

~~Fig. 6a~~ Fig. 4a shows that the location of the energetic maximum moves upslope when changing the width function from divergent (*div*), over parallel (*const*) to convergent (*conv*). The magnitude of the absolute value of the maximum increases in a similar fashion. The distribution of geopotential from top to bottom clearly influences the location and size of maxima ~~(Fig. 6b). Interestingly a hillslope with a negative exponential form,~~(Fig. 4b). Hillslope profiles which ~~is morphologicallyare~~ formed by soil creep (SC) show the ~~youngest, has by far~~maximum of E_f^{pe} farthest downslope, whereas profiles related to rainsplash (RS) and soil wash (SW) erosion reach the ~~largest~~maximum potential energy ~~maximum and therefore highest geopotential difference with~~farther upslope. As potential energy has dissipated at the end of the hillslope, this implies that SC profiles dissipate more energy on shorter flow path distance than RS or SW profiles (indicated by the gradient of E_f^{pe} in Fig. 4b). If dissipation is proportional to bed stress (see discussion in sect. 2.3) this means that for the same amount of energy input across the hillslope ~~end. Larger differences mean more available potential energy to perform work within the specified hillslope distance, which might result in enhanced erosion~~ larger bed stresses occur on SC profiles while in comparison ~~to e.g. sinusoidal or exponential hillslope forms. In line with this idea about morphological ages is also the growth of energy gradients from exponential and sinusoidal~~SW profiles relate to ~~negative exponential (old, smaller gradients to young, larger gradients).~~ lower relative bed stress.

Similarly, an increasing rainfall infiltration excess intensity I increases the magnitude of the energy maxima while it does not affect their location ~~(Fig. 6c~~(Fig. 4c). Increasing energy maxima imply steeper energy gradients resulting in more power during the energy conversion processes. We thus state that the distribution of potential energy in space as a function of hillslope width, form and rainfall intensity and seems to go hand in hand with the morphological stages of hillslope forms.

~~The analysis of hillslopes that accumulate rainfall and also experience a significant upslope runon (Fig. 5d) revealed that the distribution of potential energy resembles much more a river's steady state with a continuously negative gradient (see Appendix B). The energetic dynamics of a hillslope with significant runon is therefore different to a hillslope with very little to no upslope runon.~~

3.3 ~~Spatial patterns~~Topographic control of ~~stream power~~

~~In a second step, we calculated stream power D_f (Eq. 5) per unit flow length in watt per meter (Fig. 7) as well as per unit area $D_{f,A}$ ($D_{f,A} = D_f/B$) in watt per square meter (Fig. 8) and plotted the resulting spatial distributions to the climatic-topographic combinations as shown in Fig. 5a, b, and c (no runon is considered here).~~

~~**For all hillslope forms, our calculations show that compared to a constant width, a converging width function increases D_f and a diverging width function decreases D_f (Fig. 7a). If more rainfall falls at higher geopotentials (converging widths), the available potential energy to be converted is larger than on hillslopes with diverging widths, which accumulate the larger share of runoff at the lower end. We also note in Fig. 7a that a converging width results in a limitation of the growth of power per unit length in contrast to diverging and constant widths, which increase power due to the additional mass input in downslope direction. Fig. 7b shows how the geopotential distribution $z(x)$ influences D_f. Exponential and sinusoidal distributions result in a point along the flow path where** energy conversion ~~**is maximized, whereas negative exponential and linear distributions unlimitedly increase power in downslope direction. For hillslope forms with a power limitation (sinusoidal, exponential) converging widths lead to a power maximum that is relatively farther upstream than it is the case for diverging widths. Fig. 7c reveals that the rainfall intensity merely has a linear scale effect on the magnitude of D_f and does not influence its relative spatial distribution.**~~rates

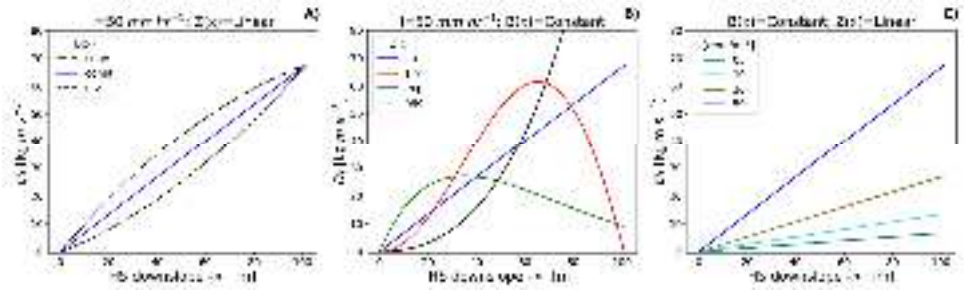

~~Figure 7: Spatial distribution of stream power D_f per unit flow length [W m^{-1}]; a) Rainfall intensity 50 mm hr^{-1} and linear~~To estimate the relative amount of influx energy that is converted into the energy balance residual D_f we compute for each hillslope form ~~but varying hillslope widths (constant, converging, diverging); b) Rainfall intensity 50 mm hr^{-1} and~~the accumulated energy residual $D_f^{acc}(xl) = \int_{x=0}^{xl} D_f(x)dx$ (watt) divided by accumulated steady state energy input $J_{in}^{acc}(xl) = \int_{x=0}^{xl} J_{Peff,net}^{pe}(x)dx$ (watt) along the flow path:

$$\frac{D_f^{acc}(xl)}{J_{in}^{acc}(xl)} = \frac{J_{f,net}^{pe,acc}(xl) + J_{in}^{acc}(xl) + J_{f,net}^{ke,acc}(xl)}{J_{in}^{acc}(xl)} \quad (12)$$

If no other mass affecting processes are considered, $J_{in}^{acc}(xl)$ is the accumulated energy influx due to rainfall at flow path distance xl. Further we do not consider upslope runon at the hillslope top in steady state $J_{f,net}^{pe,acc}(xl) = -J_{f,out}^{pe}(xl) = -\rho Q(xl)h(xl)g$ and $J_{f,net}^{ke,acc}(xl) = -J_{f,out}^{ke}(xl) = -\rho Q(xl)v(xl)^2/2$ so that Eq. (12) becomes:

$$\frac{D_f^{acc}(xl)}{J_{in}^{acc}(xl)} = 1 - \frac{J_{f,out}^{pe}(xl) + J_{f,out}^{ke}(xl)}{J_{in}^{acc}(xl)} \quad (13)$$

Equations (12) and (13) describe at each point along the flow path how much energy of the upslope accumulated potential energy from rainfall is neither conserved as kinetic nor potential energy of the mean flow. The ratio D_f^{acc}/J_{in}^{acc} is therefore a thermodynamic descriptor that can be used to estimate the dissipation per power, i.e., energy input, independent of absolute flow path lengths, rainfall rates and geopotential gradient. Similarly, the ratio $J_{f,out}^{ke}/J_{in}^{acc}$ describes the relative magnitude of upslope accumulated input energy that is converted into kinetic energy at each cross section along the flow path.

Formatted: Heading 2

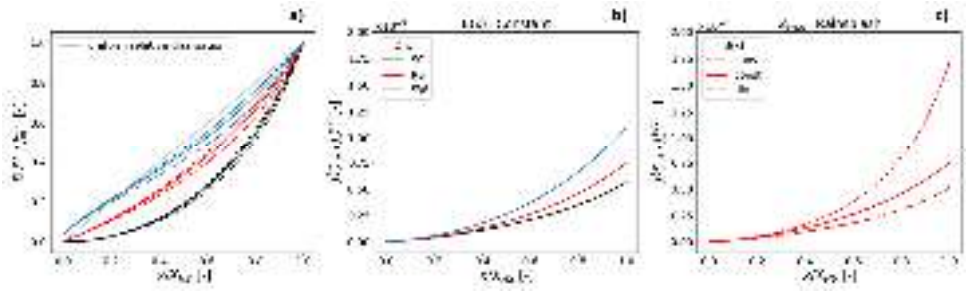

Figure 5: Spatial distribution of the ratio of a) accumulated dissipation and accumulated energy influx; b) kinetic energy outflux and accumulated energy influx for constant hillslope width but varying hillslope forms ~~(linear, sinusoidal, exponential, negative exponential); Linear~~ ; c) kinetic energy outflux and accumulated energy influx for hillslope form ~~and constant~~ related to rainsplash but varying hillslope width ~~but varying rainfall intensities;~~distributions.

~~While stream power per unit length represents macroscopic energy dynamics of the whole hillslope and therefore total energy, stream power per unit area is related to forces that act locally on soil material. Fig. 8a shows the distribution of unit stream power $D_{f,A}$ (in watt per square meter) for the different width functions (compare Fig. 5b) of a hillslope with linear distribution of geopotential. In contrast to a constant width, diverging widths decrease stream power per unit area and converging width increase $D_{f,A}$ in downslope direction. Although the additional mass per unit area for converging widths decreases in downslope direction, flow accumulation leads to larger water depths and therefore more power per unit area. It should be noted, that at the hillslope outlet, total stream power (Fig. 7a) is equal for all hillslope width functions, while stream power per unit area is clearly different (Fig. 8a). $D_{f,A}$ of the considered geopotential distributions is shown in Fig. 8b, mirroring a scaled distribution of total stream power (Fig. 7b), which indicates that while the distributions of D_f and $D_{f,A}$ are controlled by energy gradients, the magnitude of macroscopic stream power is controlled by hillslope width functions and therefore flow accumulation. A hillslope which is accumulating more flow along the same distance has larger stream power than a hillslope with less flow accumulation, however both hillslopes might in total dissipate the same amount of energy for the same flow length. Similarly, rainfall intensity has just a scale effect on $D_{f,A}$ but does not influence its relative spatial distribution (Fig. 8c).~~

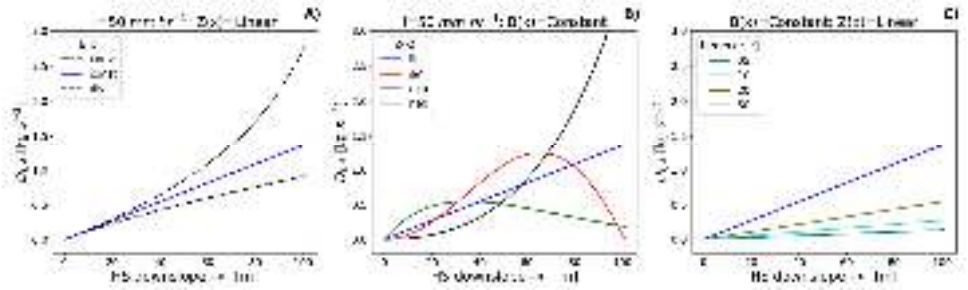

~~**Figure 8: Spatial distribution of stream power $D_{f,A}$ per unit flow area [W m^{-2}]; a) Rainfall intensity 50 mm hr^{-1} and linear hillslope form but varying hillslope widths (constant, converging, diverging); b) Rainfall intensity 50 mm hr^{-1} and constant hillslope width but varying hillslope forms (linear, sinusoidal, exponential, negative exponential); Linear hillslope form and constant hillslope width but varying rainfall intensities;**~~

Fig. 5a reveals a distinct pattern of D_f^{acc}/J_{in}^{acc}. For SW hillslope forms the ratio is continuously larger than for RS and SC forms. Regardless of absolute energy influx, SW hillslope forms convert relatively more influx energy into D_f than RS or SC forms. Similarly, but to a much smaller degree than profile form, hillslopes with converging widths dissipate relatively more energy on less flow path lengths compared to constant or diverging widths. For all forms, J_{in}^{acc} is almost completely dissipated at the end of the hillslope ($D_f^{acc}(X_{HS}) \approx J_{in}^{acc}(X_{HS})$) and only a minor part of J_{in}^{acc} is converted into kinetic energy (Fig.5b and c: $J_{f,out}^{ke}/J_{in}^{acc} < 0.002$). SW hillslope forms convert a larger part of the influx energy into kinetic energy than RS and SC forms

and the same hierarchy is found in converging, to constant and to diverging hillslope widths (Fig. 5c). The function of kinetic energy along the flow path is convex, which relates to increasing production of kinetic energy per energy influx.

3.4 Discussion

In this section we related the spatial distribution of slope (hillslope form) to the distribution of potential and kinetic energy of surface runoff. As form is also connected to the dominant erosion process, an analysis of energy dissipation provides a link between erosion process and thermodynamic principles. In a first step we digitized surface runoff experiments by Emmett (1970) and we showed that the distribution of potential energy results in a distinct flow path distance with maximum potential energy. Up to this point the system net accumulates energy and only undergoes a net loss of energy after this location. The distribution of these zones of energy production and energy depletion seems to be related to the transition of the system from one type of flow regime to another. Magnitude and distribution of energy are relative to a level of null energy at the hillslope end, and therefore represent an assumed equilibrium state of the land-water system at the hillslope scale. From a larger perspective the accumulated discharge at the end of the hillslope can perform work within the context of the whole catchment, which has been discussed previously (cf. Rodriguez-Iturbe et al., 1992; Kleidon et al., 2013).

For an analysis of these equilibrium state hillslopes, we relied on established semi-empirical descriptions of hillslope forms and related erosion processes (Kirkby, 1971) and we assumed that surface runoff on equilibrium hillslopes has dissipated all potential energy at the downslope end (usually the channel bank). The resulting steady state distribution of potential energy of surface runoff was then calculated by a friction law that was established for stony hillslopes in Arizona (Nearing et al., 2017) but in essence expresses the tendency of a hillslope surface to spatially organize friction as a function of slope and has previously been established with different parameters for rill flow (Govers, 1992). We note that these studies were concerned with surfaces which had little to no vegetation influencing the resistance to erosion of the soil particles, meaning that morphological adaptations were predominantly due to surface runoff. In a similar fashion we did not account for vegetation and infiltration but should mention that these processes would certainly affect the here presented steady state energy balance and its residual. Therefore, we stress that the presented distribution of potential energy is meant to approximate steady state runoff on equilibrium hillslopes with respect to frictional adaptation without vegetation and situations with significant infiltration excess runoff.

The resulting distributions reveal that on hillslope forms which relate to diffusive erosion (SC slope forms), $E_f^{pe,max}$ of surface runoff is found farther downslope, but with relatively larger magnitude than for forms related to advective erosion (SW). The net energy depletion zone on SC slopes depletes therefore for the same runoff more energy on shorter flow path distance than SW or RS slope forms, which implies larger bed stress.

Energetically, this can be expressed as relative accumulated dissipation per energy influx D_f^{acc}/J_{in}^{acc}. Interestingly we find that hillslope forms that relate to soil wash convert a larger part of the energy influx into D_f than RS and SC related forms. This means that although absolute bed stress is larger for SC formations, SW forms maximize work per input energy, and are therefore more dissipative in relative terms. This makes sense as D_f incorporates energy needed for sediment detachment and transport and is in line with the theory that SW forms maximize kinetic energy per energy influx (Leopold and Langbein, 1962). From a thermodynamic perspective this corresponds to an increase of entropy, as energy can be distributed across more energetic states if the ratio D_f^{acc}/J_{in}^{acc} is larger. Similarly, the distribution of the derivative of D_f^{acc}/J_{in}^{acc} is almost uniform for SW forms (cf. grey, straight line in Fig. 5a), which relates to the equal energy expenditure hypothesis of optimal channel networks (Rodriguez-Iturbe et al., 1992), as well as to a constant production of entropy per unit discharge (Leopold and Langbein, 1962).

Our assessment is based on an empirical relation between flow velocity and unit discharge and therefore does not provide closure to the energy balance. However, the Eq. (6) implicitly incorporates a spatial organization of relative friction (cf. sect. 2.2) which in accordance with our results seems to be supported by thermodynamic theory. Reversely, we show that maximum

power and equal energy expenditure per unit discharge for surface runoff on hillslopes should result in friction laws like the ones proposed by Govers (1992) and Nearing et al. (2017). In fact, the proposed slope-velocity equilibrium by Nearing et al. (2005) seems to be a natural outcome of the equal energy expenditure, maximum power and maximum entropy concepts.

Finally, we want to point out that along a similar line of thoughts Hooshyar et al. (2020) have recently shown that logarithmic mean elevation profiles of landscapes resemble the logarithmic mean velocity profile in wall bounded turbulence. The authors concluded that these logarithmic profiles are a consequence of dimensional length-scale independence, and therefore apply to different dynamical systems, possibly also to the much smaller hillslope scale. As these profiles were observed at an intermediate region and therefore are spatially transient, we believe they might relate to the here proposed transition from energy production to energy depletion, inspired by the well-known energy cascade of turbulent kinetic energy (Tennekes and Lumley, 1972).

4 Numerical simulation of overland flow experiments and their micro-topographic controls on distributed energy dynamics

We now explore the spatial distribution of potential energy in sheet and rill overland flow ~~within~~, which was observed during rainfall-runoff experiments carried out in the Weiherbach catchment (Gerlinger, 1996). Therefore, we ~~build~~built an extension to the physical hydrological model Catflow, which allows the accumulation of flow from sheet flow areas into rills (Catflow-Rill). As these experiments were performed on 12 m plots with a uniform slope they correspond to the rain-splash dominated hillslope type, as shown in Fig. 3b.

4.1 Study area and experimental data base

The Weiherbach catchment is an intensively cultivated catchment which is almost completely covered with loess up to a depth of 15 m (Scherer et al., 2012). It is located in the Kraichgau region northwest of Karlsruhe in Germany. Because of the hilly landscape, the intensive agricultural use and the highly erodible loess soils, erosion is a serious environmental problem in the Kraichgau region. The Weiherbach itself has a catchment area of 6.3 km^2 and is around 4 km long. Elevation ranges from 142 m to 243 m above sea level; the slopes are long and gentle in the west, and short and steep in the eastern part of the catchment. The climate is semi-humid with a mean annual temperature of 10 °C (Scherer, 2008). More than 90 % of the catchment area is arable land or pasture, 7 % are forested and 2.5 % are paved (farmyards and roads). Severe runoff and erosion events are typically caused by thunderstorms in late spring and summer, when Hortonian overland flow dominates event runoff generation (Zehe et al., 2001). A comprehensive hydro-meteorological dataset as well as data on soil hydraulic properties, soil erosion, tracer and sediment transport are available for the Weiherbach (Scherer et al., 2012; Schierholz et al., 2000).

Here we ~~use 2 selected characteristic~~analyse 31 rainfall simulation experiments (Gerlinger, 1996; cf. supplemental data), which were performed to explore formation of overland flow and the erodibility of the loess soils (Scherer et al., 2012). The rainfall simulators were designed to ensure both realistic rainfall intensities and kinetic energies on plots of 2 m by 12 m size. Rainfall intensity of ~~both~~ experiments ~~was set~~ ranged between 34.4 to 62.4 mm h^{-1}. ~~Rainfall simulation was stopped when overland flow and sediment concentration had reached steady state.~~ Runoff and sediment concentrations in overland flow samples were derived from samples taken during the experiments. We categorized an experiment as reaching steady state discharge if during the last time quarter, the relative change of discharge between measurements stays below 10% measurement error (Fig. 6a). Likewise, we proceeded to classify measured sediment concentrations (Fig. 6b). The final steady state classification of each experiment per discharge and sediment concentration can be found in the supplemental data to this study. All but 5 experiments were classified as reaching steady state discharge (Fig. 6a) while only 9 were classified as reaching steady state sediment concentrations (Fig. 6b). This means that only experiments which reached steady state runoff as well as sediment concentrations can be considered as being truly in an energetic steady state (7 out of 31, cf. supplemental data). The different sites were characterized according to their antecedent soil moisture, soil texture and organic content in the upper 5-10 cm

(Scherer et al., 2012). Additionally, surface roughness (Manning's n) was estimated from the falling limb of the observed hydrograph (Engman, 1986; Govers et al., 2000). ~~For the two selected experiments (lek_2 and oek2_4), antecedent soil moisture of the plots was 25.6 and 18.4 Vol%, organic content1.9 and 2.5 %, clay content 16.8 and 21.1 % and Manning's n 0.045 and 0.032 s $m^{-1/3}$.~~Observed rill flow velocities $v_{RF,obs}$ were measured by upslope tracer injection and correspond to the time it took until the peak of tracer concentration reached the plot outlet, while reported sheet flow velocities $v_{SF,obs}$ have been back calculated from measured runoff rates. Further details on the experimental setup are provided by Gerlinger (1996), Seibert et al. (2011), and Scherer et al. (2012). A first analysis of the data already reveals that experimental sites with a larger Manning's n correspond to a smaller ratio $v_{rat} = v_{SF,obs}/v_{RF,obs}$, suggesting that a larger roughness leads to stronger accumulation of runoff in rills. As will be shown, this in turn relates to the portioning of kinetic energy between sheet and rill domain.

Formatted: Font: Italic

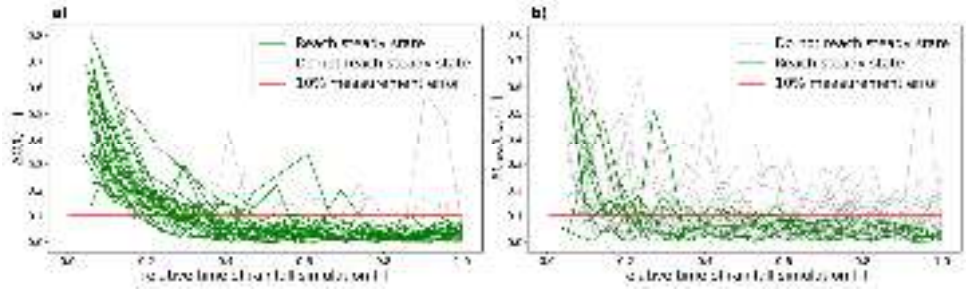

Figure 6: Classification of rainfall simulation experiments, green lines reach steady state during 0.75-1.0 of relative time of rainfall simulation: a) Relative change of discharge; and b) Relative change of sediment concentration

4.2 Model and model setup

~~In order to analyse total spatial distribution of energy and dissipation we present here~~Next, we present an extension to the Catflow model (Zehe et al., 2001), accounting for a dynamic link between sheet- and rill flow of ~~Hortonian~~ surface runoff. The model has previously been extended, incorporating water-driven erosion (Scherer, ~~2007~~2008) and has been shown to successfully portray the interplay of overland flow, preferential flow and soil moisture dynamics from the plot to small catchment scales (Graeff et al., 2009; Loritz et al., 2017; Zehe et al., 2005, 2013).

A catchment is represented in CATFLOW by a set of two-dimensional hillslopes (length and depth), which may be connected by a river network. Each hillslope is discretized using curvilinear orthogonal coordinates; the third dimension is represented by a variable width. Subsurface water dynamics are described by Richards' equation, which is solved numerically by an implicit mass-conservative Picard iteration scheme. The simulation time step for soil water dynamics is dynamically adjusted to achieve an optimal change of the simulated soil moisture, which assures fast convergence of the Picard iteration. Soil hydraulic properties are usually parameterized using the van Genuchten-Mualem model (Mualem, 1976; van Genuchten, 1980), but other options are available. Enhanced infiltrability due to activated macropore flow is conceptualized through enlarging the soil hydraulic conductivity by a macroporosity factor f_{mak}, when a soil moisture threshold is exceeded. This approach is motivated by the experimental findings of Zehe and Flühler (2001a and 2001b) in the Weiherbach catchment and has been shown to be well suited for predicting rainfall-runoff dynamics (Zehe et al., 2005) as well as tracer transport at the plot and the hillslope scales (Zehe and Blöschl, 2004; Zehe et al., 2001).

4.2.1 Representation of overland flow in Catflow and Catflow-Rill

Overland flow is simulated in Catflow-Rill with the diffusion wave equation, which is numerically solved using an explicit upstreaming scheme, a simplification of the Saint-Venant equations for shallow water flow, for details of the numerical scheme

we refer to Scherer (~~2007~~2008). Flow velocity is calculated with Manning's equation (Eq. ~~7).~~(5)). The previous Catflow model assumes sheet flow only. To incorporate a rill domain that dynamically interacts with sheet flow, we conceptualise the hillslope surface similar to the open book catchment (Wooding, 1965) as an open book hillslope ~~(Fig. 9).~~(Fig. 7). In this configuration water may accumulate in a trapezoidal rill of width B_r in the middle of the open book hillslope with width B_{HS} and downslope length L_{HS}. Rainfall is added proportionally to the projected area along the flow path in both domains, resulting in spatially distributed sheet flow Q_{SF} and rill flow Q_{RF}. The link is established by a flow accumulation coefficient ~~c_{FC}~~ C_f (Eq. ~~12).~~(14)). This is visualized in ~~Fig. 9~~7 by the angle γ (in radians) between the vectors $\overrightarrow{Q_{SF}}$ and $\overrightarrow{Q_{RF}}$, which manifest at each point on the sheet flow surface the tendency of a volume water to flow downslope the hillslope gradient α or to follow the secondary flow accumulation gradient β (Eq. ~~12).~~(15)).

$$dQ_{link}(x) = Q_{SF}(x) \text{ ~~$* c_{FC}$~~} \times C_f(x) \quad (~~12~~14)$$

$$tan(\gamma) = \frac{|\overrightarrow{Q_{RF}}|}{|\overrightarrow{Q_{SF}}|} = \frac{\alpha}{\beta} \quad (~~13~~15)$$

The maximum amount of flow which is transferred per unit flow path length from the sheet domain into the rill domain is then given by:

$$~~c_{FC,max}~~ C_{f,max} = \gamma ~~* \frac{2}{\pi}~~ \times \frac{2}{\pi} \quad (~~14~~16)$$

However, depending on the configuration of the open book hillslope, we need to account for a flow path length L_{FC}, where flow accumulation becomes constant and maximum:

$$L_{FC} = B_{HS} ~~* tan(\gamma)~~ \times tan(\gamma) \quad (~~15~~17)$$

From hillslope top to the flow path length L_{FC}, the flow accumulation coefficient is linearly interpolated between ~~$c_{FC}(x = 0)$~~ $C_f(x = 0) = 0$ until ~~c_{FC}~~ $C_f(x = L_{FC}) =$ ~~$c_{FC,max}$~~ $C_{f,max}$.

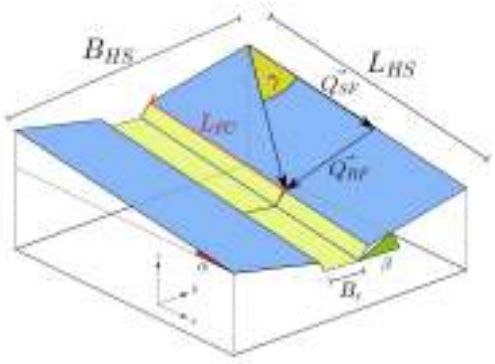

Figure ~~9:~~7: Representation of overland flow domains in Catflow-Rill as open book hillslope: Sheet flow domain (blue area) and Rill flow domain (yellow area).

4.2.2 Model setup and calibration of flow accumulation

From the experimental database Scherer et al. (2012) created Catflow simulation setups, which were calibrated to reproduce runoff by adapting the macroporosity factor to scale infiltration capacity. The hillslopes were parameterized and initialized using observed data on average topographic gradient, plant cover, soil hydraulic functions, surface roughness, soil texture, and antecedent soil moisture. The models were driven by a block rain of the respective intensity and duration of the experiment. ~~For calibration with the here presented extension Catflow-Rill (see previous section), we chose 2 characteristic experiments with similar slope and equal rainfall intensities of 62.4 mm h^{-1}. For experiment "lek_2" (slope=0.163 m m^{-1}) significant rill flow was reported (Gerlinger, 1996) with steady state rill runoff velocities ($v_{RF,obs} = 0.239\ m\ s^{-1}$) almost double the average sheet flow velocities ($v_{SF,obs} = 0.122\ m\ s^{-1}$). The reported rill velocities were measured by upslope tracer injections and correspond to the time it took until the peak of tracer concentration reached the plot outlet. Contrarily, during experiment "oek2_4" (slope=0.151 m m^{-1}) little to no rill flow was observed, manifesting in almost equal surface runoff velocities of $v_{SF,obs} = 0.142\ m\ s^{-1}$ and $v_{RF,obs} = 0.15\ m\ s^{-1}$. From here onwards subscript "obs" relates to measured, reported values from the referenced experimental studies and subscript "sim" relates to the results of the presented calibrated numerical simulations. Both hillslopesHillslopes were discretized on a 2D numerical grid with an average lateral distance of 60cm60 cm and vertically increasing distances starting with 1cm1 cm at the surface and ending with 5cm5 cm on the soil bottom. This resulted in 21 x 29 computationcomputational points for both 12m12 m long, 2m2 m wide and 1m1 m deep hillslope plots. Manning's n was determined during the experiments (Gerlinger, 1996) as 0.045 s m$^{-1/3}$ for "lek_2" and 0.032 s m$^{-1/3}$ for "oek2_4". Soil hydraulic parameters of the Van Genuchten-Mualem model were reported by Schäfer (1999), who conducted a soil hydraulic parameter campaign within the Weiherbach catchment and classified five homogeneous soil types. From these, parameters from the C-horizon of Pararendzinacalcaric regosol soil type were used for the presented simulations (Scherer, 20072008) in accordance towith the location of the experimental plots within the catchment (see Table 31). Grain size distributions are available for plot experiment "lek_2", which consist of 15% clay, 78% silt and 7% sand, with mean particle diameter $d_{...}$diameters d_{50} between 20 to 3070 µm (Scherer, 20072008; supplemental data).~~

Table 1: Soil hydraulic parameters of Van Genuchten-Mualem model for simulated hillslopes, namely saturated hydraulic conductivity k_s, saturated soil moisture θ_s, residual soil moisture θ_r, reciprocal air entry point α_s, as well as soil hydraulic form parameters n_s and γ_s

	$k_s\ [m\ s^{-1}]$	$\theta_s\ [m^3\ m^{-3}]$	$\theta_r\ [m^3\ m^{-3}]$	$\alpha_s\ [m^{-1}]$	$n_s\ [-]$	$\gamma_s [-]$
~~Paradenzina~~Calcaric regosol	6.803*10^{-7}	0.444	0.066	0.51	2.24	0.71

To ~~calibrate~~match the observed flow velocities, we adjusted the flow accumulation coefficient ~~c_{FC}~~C_f, starting at 0.001 and incrementing in 0.001 steps, compared the steady state values of $v_{RF,sim}$ and $v_{RF,obs}$ and stopped the incrementation of . ~~For each calibration run we compared the steady state values of $v_{RF,sim}$ and $v_{RF,obs}$ and stopped the incrementation of $c_{FC}C_f$~~ when the residual of both values was below 1% of $v_{RF,obs}$.

~~**4.3 Simulation results**~~

4.3. (cf. Fig. 8b and d). Fig. 8 shows the result of selected calibration iterations for the representative experiments "lek_2" and "oek2_4" to highlight the sensitivity to flow accumulation. For experiment "lek_2" (slope=0.163 m m^{-1} ~~Catflow~~) significant rill flow was reported (Gerlinger, 1996) with steady state rill runoff velocities ($v_{RF,obs} = 0.239$ m s^{-1}) almost double the average sheet flow velocities ($v_{SF,obs} = 0.122$ ~~results~~

m s^{-1}). Contrarily, during experiment "oek2_4" (slope=0.151 m m^{-1}) little to no rill flow was observed, manifesting in almost equal surface runoff velocities of $v_{SF,obs} = 0.142$ m s^{-1} and $v_{RF,obs} = 0.15$ m s^{-1}. For both hillslopes ~~under consideration~~ the

Formatted: Superscript

calibration produced good results after few ~~steps of~~ incrementing ~~the flow accumulation coefficient.~~steps. For "lek_2" this resulted in $c_{FC}C_f = 0.018$ and for "oek2_4" in $c_{FC}C_f = 0.0032$ ~~(Fig. 10a~~(Fig. 8a and c). Total mass is conserved as total simulated discharge $Q_{tot,sim}$ ($Q_{tot} = Q_{RF} + Q_{SF}$) stays constant independent of $c_{FC}C_f$ for all simulations, ~~equalling~~while discharge in the ~~observed discharges (Scherer et al., 2012).~~rill domain grows with C_f. Except for the onset of surface runoff, $Q_{tot,sim}$ stays with 10% error tolerance bands of measured total discharge $Q_{tot,obs}$ for both experiments (compare ~~Fig. 10a~~Fig. 8a and c grey bands). ~~The here presented Catflow-Rill simulations divide total surface runoff into simulated~~While the observed rill flow velocities are matched well for both sites (lek_2 $v_{RF,sim}$ =0.238 m s^{-1}, oek2_4 $v_{RF,sim}$= 0.15 m s^{-1}), computed sheet flow ~~$Q_{SF,sim}$ and rill flow $Q_{RF,sim}$, computing higher discharges in the rill domain with increasing flow accumulation coefficient. For lek_2, the final rill flow velocity resulted in 0.238 m s^{-1} and for oek2_4 in 0.15 m s^{-1}, matching~~velocities exhibit small deviations from the observed values ~~0.239 m s^{-1} for lek_2 and 0.15 m s^{-1} for oek2_4 (Fig. 10b and c). Computed sheet flow velocities are close to observed steady state results but not as a precise match as calibrated rill flow velocity.~~ One reason might be the ~~measurement~~ approach to calculate of ~~sheet flow, which was done by indirect calculation of~~ v_{SF} ~~through~~indirectly from measured total discharge and v_{RF} (Gerlinger, 1996), and ~~therefore is~~the likely ~~to produce~~ larger measurement errors. The final simulated steady state value of v_{SF} is however for both experiments within a 10% error margin, which is tolerable in the light of measurement uncertainty.

Formatted: Keep with next

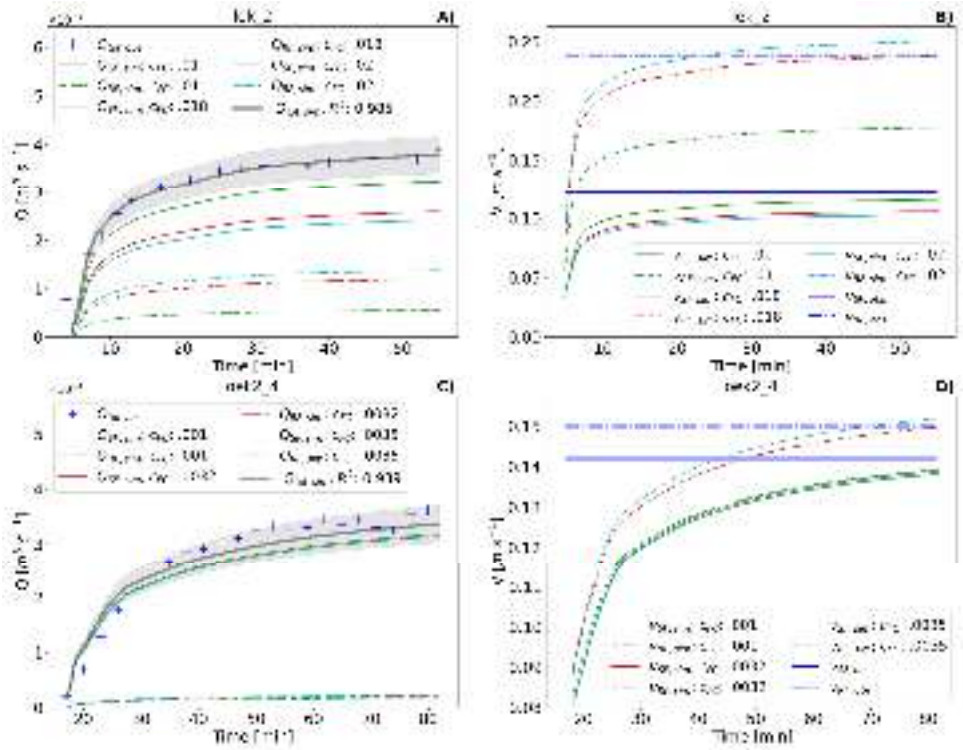

Figure ~~10:~~8: Results of calibrations runs for ~~both~~ experiments "lek_2" and "oek2_4": a) and c) Calibrated total discharge $Q_{sim,tot}$, measured discharge $Q_{tot,obs}$ (incl. grey 10% error band) and computed contributions of sheet flow $Q_{SF,sim}$ and rill flow $Q_{RF,sim}$; b) and d) Observed rill and sheet-flow velocities $v_{RF,obs}$ and $v_{SF,obs}$ and calibration runs for different flow accumulation ~~coefficient c_{FC}~~coefficients C_f

4.3 Simulation results

4.3.2 Distribution1 Flow accumulation in rills

Figure 9 shows that calibrated rill flow velocities match the observed values for all 31 experiments well (Fig. 9a). We also note that magnitude of rill flow velocity is correlated to flow accumulation, ranging from smallest $v_{RF,obs} = 0.11$ m s^{-1}, $C_f = 0.002$ to largest $v_{RF,obs} = 0.3$ m s^{-1}, $C_f = 0.024$. In line with the observations, simulated rill flow velocities are not correlated to slope (Appendix B, Fig. B4). The resulting $v_{SF,sim}$ are close to observed sheet velocities, with 23 out of 31 lying within 10 % measurement error (Fig. 9b, grey band). Outliers can partly be explained by classification of experiments reaching steady state runoff Q^{SS} and/or steady state sediment concentrations C_{Sed}^{SS} (cf. sect. 4.1 Fig. 6) and experiments which should be considered not steady state (Q^{NSS} and/or C_{Sed}^{NSS}, compare Fig. 9b). Simulations with largest inconsistency between $v_{SF,sim}$ and $v_{SF,obs}$ are either classified as Q^{NSS} (Fig. 9b, marker "x") or C_{Sed}^{NSS} (Fig. 9b, coloured red), or both. In general, the proposed flow accumulation model slightly underestimates sheet flow velocities. Finally, we find a strong correlation between C_f and the ration of sheet to rill flow velocity $v_{rat} = v_{SF,sim}/v_{RF,sim}$ (Fig. 9c), which can be represented as a power law $v_{rat} = 0.11 * C_f^{-0.38}$ ($R^2 = 0.82$). In parallel we also find that Manning's n is positively correlated to C_f as well as v_{rat} (cf. Fig. 9c and Appendix B). Largest friction coefficients are therefore related to highest flow accumulation but lowest v_{rat} values.

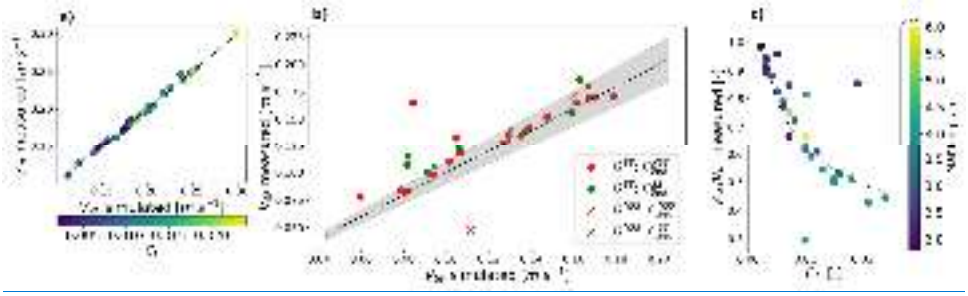

Figure 9: Results of calibration of flow accumulation to observed rill flow velocities: a) $v_{RF,sim}$ vs. $v_{RF,obs}$; b) $v_{SF,sim}$ vs. $v_{SF,obs}$; and c) C_f vs. $v_{rat} = v_{SF,sim}/v_{RF,sim}$

4.3.2 Dissipation and erosion

In a similar fashion to comparison of relative dissipation along the typical hillslope profiles in sect. 3.3, we calculate the kinetic energy export at the hillslope end in relation to the potential energy influx by rainfall and compare the relative contributions of rill flow and sheet flow. However, we can only confidently evaluate this for simulated experiments, which can be classified as steady state (for discharge and sediment concentrations; cf. Fig. 6) and where $v_{SF,sim}$ matches $v_{SF,obs}$ sufficiently well (Fig. 9b). Considering all these requirements results in only 5 out of 31 simulations for which we can confidently compare relative dissipation rates to potential energy influx by rainfall as defined in Eq. (18). Consequently, as we analyse energy relative to hillslope outlet, potential energy is assumed to be completely dissipated or exported as kinetic energy at the hillslope end, so that Eq. (13) can be written as:

$$\frac{D_f^{acc}}{J_{in}^{acc}} = 1 - \frac{J_{f,out}^{ke}}{J_{in}^{acc}} \quad (18)$$

J_{in}^{acc} implicitly incorporates rainfall intensity, slope and area of the hillslope and normalizes dissipation rates for comparison among the selected experiments. Fig. 10a plots $J_{f,out}^{ke}/J_{in}^{acc}$ for the 5 trusted experiments (marked as "+", high confidence) as well as for the 26 remaining simulations (marked as circle, low confidence). For each simulation we plotted the relative contribution of sheet flow F_{SF} (blue) and rill flow F_{RF} (black) against flow accumulation coefficient, which sum up to total relative conversion rates of potential to kinetic energy. As the kinetic energy flux is proportional to Q^3 (cf. Eq. (A5) b, $J_{f,out}^{ke} =$

Formatted: Normal

$f(Q^3)$), we analytically express F_{SF} and F_{RF} as cubic functions of accumulated discharge ($F_{RF/SF}(C_f) = a_1 C_f^3 + a_2 C_f^2 + a_3 C_f + a_4$) with C_f determining Q_{RF} and Q_{SF}. Fig. 10a presents for each domain F_{RF} and F_{SF} the fitted cubic function as well as their sum, which represents the total relative rate of kinetic energy export at the hillslope outlet as function of flow accumulation in the rill domain. It is interesting to note that both functions also capture a significant portion of points which have been ruled out due to lower confidence, and consequently were not included in the fit. As F_{SF} declines and F_{RF} increases with flow accumulation, total normalized kinetic energy export exhibits a distinct minimum value for C_f values in the range of 0.011 to 0.012 (Fig. 10a). This also corresponds to the region where relative kinetic energy export of rill flow $J^{ke}_{RF,out}$ and sheet flow $J^{ke}_{SF,out}$ are equal. According to Eq. (18) this equally means that the relative dissipation rate is maximized in this range of C_f values.

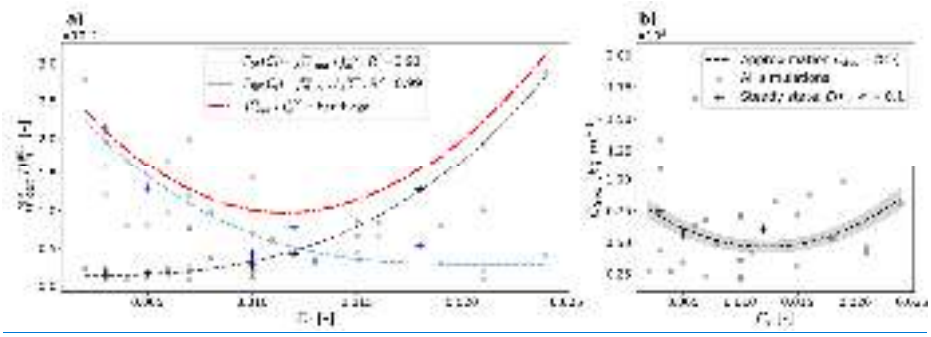

Figure 10: a) Relative flux of kinetic energy at the hillslope outlet as a function of flow accumulation for rill domain (F_{RF}) and sheet domain (F_{SF}) as well as total relative flux (F_{RF}+F_{SF}); b) Measured sediment concentrations at hillslope outlet plotted against flow accumulation parameter C_f, simulations with $Err_{SF} = |v_{SF,sim} - v_{SF,obs}|/v_{SF,obs}$ below 10% and classified steady state are marked with "+".

4.3.3 Spatial distribution of energy and flow regimes

The calibrated CATFLOW-Rill models also provide an estimate of the spatial distribution of ~~power and~~ energy for the rill- and the sheet- domains. ~~based on Q_{SF} and Q_{RF} (Fig. 11a and c) and therefore allow a comparison of spatial energy distribution of systems with high accumulation of runoff in rills and systems with little to no rill flow. Fig. 11a and Fig. 12a~~ **Error! Reference source not found.**a and b show the spatial distribution of potential energy ~~per flow length E_f [J~~ E_f^{pe} (joule m^{-1}~~]~~ ~~for~~) and kinetic energy E_f^{ke} in each domain ~~and~~for an experiment~~.~~ with significant rill flow (lek_2, cf. Fig. 8). First ~~of all~~, we note that both approaches of runoff calculation (~~Catflow and Catflow-Rill~~)$C_f = 0$ and $C_f = C_{calib}$) result in a local maximum of potential energy and that ~~more~~most energy is stored within the sheet~~ than in the rill~~ flow domain. The rill ~~simulations increases~~simulation increases potential energy within the rill domain and ~~decrease E_{pot}~~decreases E_f^{pe} in the sheet flow domain. This happens non-linearly, meaning relatively more energy is transferred from the sheet to the rill flow domain downslope than upslope. As a result, the location of maximum potential energy is shifted in upslope direction~~. As in~~ and decreases in magnitude. The accumulation of runoff in rills leads to an increase of E_f^{ke} in the rill domain and contrarily a decrease of E_f^{ke} in the sheet domain in flow direction (Fig. 11b). For the calibrated experiment lek_2 ~~rill flow is much more pronounced, this shift and the related change of potential energy is much stronger than for oek2_4. Spatial distribution of kinetic energy E_{kin} per flow length is plotted in Fig. 11b and Fig. 12b. While results of Catflow and Catflow-Rill are similar for oek2_4 (Fig. 12b), the accumulation of flow in the rill domain has large impacts for lek_2 (Fig. 11b). In comparison to the simulation without rill domain, kinetic energy decreases downslope, while in the rill flow domain E_{kin} increases downslope. Interestingly, for Catflow-Rill, the kinetic energy at the hillslope outlet of sheet flow and rill flow~~ kinetic energies of the two domains approach each other in downslope direction and are almost equal~~. The sum of both energies (E_{pot} + E_{kin}) is plotted as total free energy~~

~~E_{tot} per flow length in Fig. 11c and Fig. 12c.~~ at the hillslope end. As potential energy is up to 1000 times larger in magnitude than kinetic energy, ~~E_{tot}~~ the sum of free energies $E_f = E_f^{pe} + E_f^{ke}$ is essentially equivalent to ~~E_{pot}. The plots show~~ E_f^{pe}. We further find that the accumulation of flow in a rill reduces the total amount of energy being stored on the hillslope.

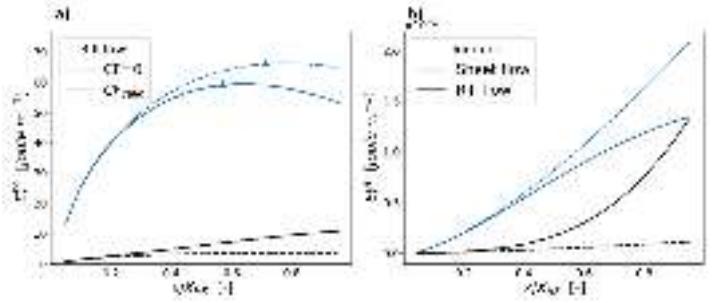

Figure 11: Spatial distribution of a) E_f^{pe} (maximum marked as ▲) and b) E_f^{ke} for calibrated rainfall runoff simulation "lek_2", separated into sheet- and rill flow

By comparing five experiments classified as steady state (cf. Fig. 10), we find that E_f^{pe} is shifted farther upslope for simulations with a) higher maximum potential energy and b) more runoff in rills (Fig. 12a). The latter becomes evident by estimation of Reynolds numbers of rill flow at the flow path length of maximum potential energy. Largest *Re* are found for energy distributions with the maximum occurring farther upslope and smallest *Re* are related to energy maxima appearing farther downslope. Computed Reynolds numbers at these maximum points range from 600 to 2100, which implies that the transition to turbulent or at least mixed flow regime is possible.

Interestingly, the ratios of kinetic energy in sheet- to rill domain declines downslope and the gradient of the curve increases (Fig. 12b) when the location and magnitude of $E_f^{pe,max}$ is moving upslope. We observed that for one out of five experiments the ratio reached unity ($E_{SF}^{ke}/E_{RF}^{ke} = 1$), while for the others kinetic energy export in the sheet domain is dominant. We can therefore conclude, that from the presented simulations only experiments with significant rill flow approached unity within the 12m plot lengths, while the plot length is too small for a final conclusion on ~~the hillslope. Also, the spatial location of the local energy maximum shifts upslope.~~experiments with less flow accumulation.

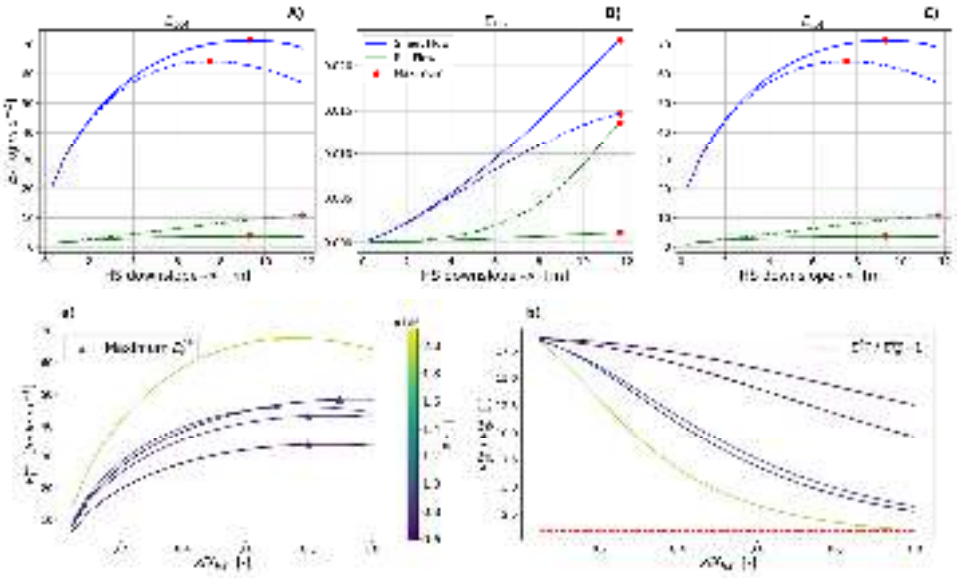

Figure ~~11: Results of Catflow-Rill~~12: Spatial distribution of a) E_f^{pe} and b) E_{SF}^{ke}/E_{RF}^{ke} for ~~no flow~~ considered experiments in the Weiherbach catchment (compare supplemental data); results are coloured by Re at hillslope distance of $E_f^{pe,max}$)

4.4 Discussion

Our approach to model the accumulation ~~($c_{IC} = 0$; solid lines) and~~ of surface runoff by a single rill and the calibration of a flow accumulation ~~($c_{IC} = 0.018$; dashed lines)~~parameter resulted in partly good approximations of observed rill and sheet flow velocities and therefore justifies the presented simplification of surface runoff across two domains. Although the model uses a single friction coefficient (Manning's *n*), which is a simplification (cf. sect. 2.2), flow accumulation in a rill and the opposite, flow dispersion of sheet flow led to spatially varying hydraulic radii, which imply variable friction along the hillslope. Manning's *n* which was determined for each experiment ~~lek_2: a) Spatial distribution of~~ (Gerlinger, 1996) is therefore closely related to flow accumulation and the ratio of sheet vs. rill flow velocity. Our results show that a larger friction coefficient leads to relatively more flow accumulation in rills, a phenomenon which was also observed in field experiments by Abrahams et al. (1990). Some of the simulations performed poorly on estimating sheet flow velocity (cf. Fig. 9b and c), this can partly be explained by classification of experiments reaching steady state discharge and sediment concentrations during the interval of rainfall simulation. Other outliers could be related to tilling, which is common on the hillslopes in the Weiherbach catchment. We conclude that for such conditions, experiments would have to be conducted for much longer durations, allowing for imprinted topographical structures of farming practices to be reversed and natural rill networks to emerge. Rieke-Zapp and Nearing (2005) applied to laboratory plots of 4 by 4 meters rainfall with maximum duration of 90 minutes and results suggest that rills have not reached an equilibrium steady state. Although the field plots have certainly been impacted by previous rain events and are therefore closer to an equilibrium state than a plane of laboratory sand, in retrospective it is not possible to judge the degree of perturbation due to farming. Nevertheless, the experiments clearly indicate that sheet- and rill flow velocity are not a function of slope but depend on flow accumulation. Lowest flow velocities were observed for simulations with lowest C_f coefficient and correlate up to largest observed flow velocity and largest calibrated C_f(Fig. 9a; supplemental data). This is in line with the postulated slope-velocity theory on hillslopes (Govers et al., 2000; Nearing et al., 2005), and to our belief, is the result of a feedback between friction coefficient and flow accumulation from sheet flow to flow in threads and then in rills.

Analysis of relative dissipation of energy per influx energy by rainfall reveals that surface runoff across rill and sheet domain is related to the existence of a maximum power state. For the analysed experiments we distinguished those which reached steady state discharge and sediment concentrations and calculated the kinetic energy per influx energy that leaves the plot. For rill flow it can be shown that kinetic energy export increases with flow accumulation, while kinetic energy of sheet flow decreases with growing C_f. As expected, kinetic energy flux of both domains can be approximated by cubic functions of C_f. The sum of both represents the total outflux of kinetic energy per potential energy ~~$\boldsymbol{E_{pot}}$; b) Spatial~~input, which is characterized by a distinct range of flow accumulation that minimizes normalized kinetic energy export. Within this range kinetic energy of both domains is approximately equal and dissipation, expressed as the energy balance residual, is maximum (cf. Fig.10a). This finding is very similar to theoretical elaborations by Kleidon et al. (2013) on surface runoff and sediment export at the catchment scale, with an accumulation of channel flow from overland flow areas in a certain number of channels. As the number of channels grows, the distance of overland flow into the channel decreases, resulting in an optimal channel number with minimum dissipation. The difference between our and Kleidon's argumentation is that tectonic uplift and the depletion of slope gradient is negligible on the small hillslope plots in the Weiherbach catchment. In contrast to the study by Kleidon et al. (2013) sediment export should therefore not be maximized but minimized, with metastable hillslopes being related to hillslopes with minimum to no erosion. An assessment of observed sediment concentrations on the experimental plots indeed seems to indicate that minimum C_{sed} might be related to minimum total kinetic energy per influx energy and therefore maximum relative dissipation (cf. Fig. 10b). In this sense the formation of rills is thermodynamically an expression of maximization of dissipation per influx energy from rainfall.

For the analysis of flow regime transitions (cf. hypothesis two), we plotted the Reynolds number of rill flow at the flow path distance where potential energy is maximum (cf. Fig. 12a). While some *Re* exceed the critical threshold for turbulence, others are below the value proposed by Emmett ($1500 < Re < 6000$). Yet, these low *Re* numbers might still relate to the onset of turbulent flow regime as reported mean particle diameters are very small ($20 < d_{50} < 70$ µm, cf. supplemental data) resulting for very shallow runoff depths in high relative roughness and consequently turbulent flow regime at lower *Re*. Although spatially distributed mean water depths were not part of the experimental data set, the results of the calibrated simulations clearly indicate that the distribution of ~~kinetic energy $\boldsymbol{E_{kin}}$; c) Spatial~~potential energy relates to the transition from laminar to turbulent flow regime in downslope direction.

Potential energy in this section is based on a relative calculation of potential energy with the null level of the 12 m plots at the outlet of the Weiherbach catchment, which makes the results (Fig. 12) comparable. We argue that surface runoff on hillslopes in its simplest case can be separated into sheet and rill flow and that the distribution of ~~total energy $\boldsymbol{E_{tot} = E_{pot} + E_{kin}}$ of individual flow domains~~flow within both domains approaches over time a maximum power state (cf. Fig. 10a). At this state dissipation per driving gradient is maximized, while the ratio of kinetic energies approach unity. We found that two of the truly steady state as well as seven other experimental sites cluster in this area. In fact, we see very strong similarities to a maximum power state of an electrical circuit where the load resistance (in the case of surface runoff: the inverse of rill conveyance) has adjusted to meet the source resistance (the inverse of sheet flow conveyance, cf. Appendix C). This finding can also be corroborated from Fig. 10a, with minimum total flux of kinetic energy being related to equal fluxes of kinetic energy (and therefore also equal kinetic energies) across both surface runoff domains.

Formatted: Normal

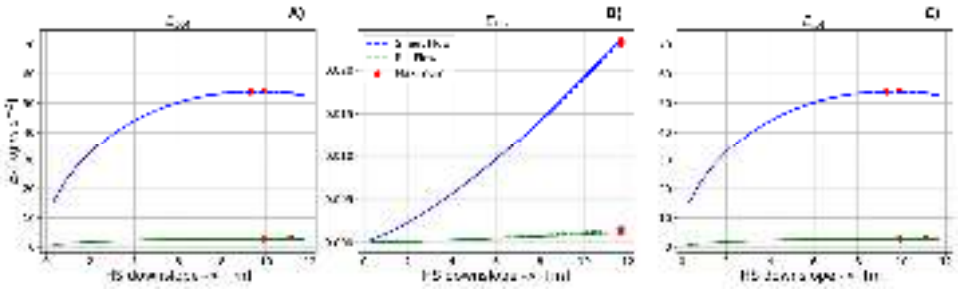

~~**Figure 12: Results of Catflow-Rill for no flow accumulation ($c_{FL} = 0$; solid lines) and with flow accumulation ($c_{FL} = 0.0032$; dashed lines) for experiment oek2_4 2: a) Spatial distribution of potential energy E_{pot} ; b) Spatial distribution of kinetic energy E_{kin}; c) Spatial distribution of total energy $E_{tot} = E_{pot} + E_{kin}$ of individual flow domains**~~

980 ~~**4.3.3 Power and erosive force**~~

~~From the Catflow and Catflow-Rill simulations we computed stream power per unit length D_f [W m^{-1}] (Eq. 5) and per unit area $D_{f,A}$ [W m^{-2}] ($D_{f,A} = D_f/b$) as well as bed stress τ [N m^{-2}] (Eq. 6). Rill flow accumulation leads to larger D_f and $D_{f,A}$ values within the rill domain and decreases both within the sheet flow domain (Fig. 13a and b; Fig. 14a and b). This result is much more pronounced for simulation of lek_2 due to the stronger rill flow component than for oek2_4. Simulation of oek2_4~~
985 ~~shows little to no difference in power per unit length between the implementation with and without rill (Fig. 14a), yet power per unit area is clearly larger in the rill- than in the sheet flow domain (Fig. 14b). Similar results are found for bed stresses (Fig. 14c and Fig. 14c). Computation of surface runoff accumulation in a rill leads to larger forces per unit area within the rill- and a lower τ within the sheet flow domain. For the soils of the experiments lek_2 and oek2_4 erosion resistance factors f_{ero} of 1.636 N m^{-2} (lek_2) and 0.826 N m^{-2} (oek2_4) were measured (Gerlinger, 1996), which we plotted as horizontal line in Fig.~~
990 ~~13c and Fig. 14c. Interestingly, the effect on bed stress of rill flow in comparison to sheet flow for lek_2 becomes significant at the flow length where τ exceeds f_{ero} (Fig. 13c).~~

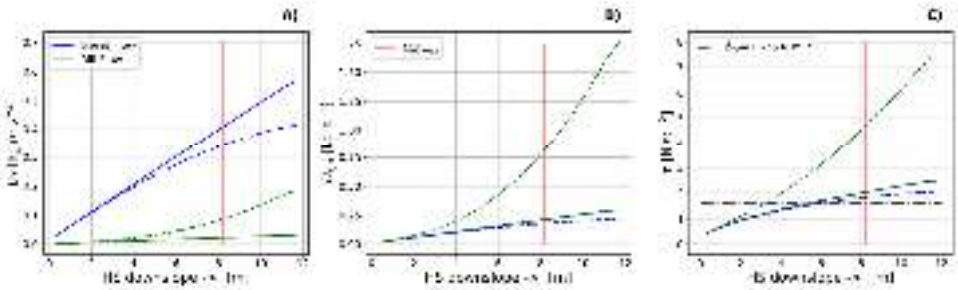

~~**Figure 13: Results of CATFLOW-RILL for no flow accumulation ($c_{FL} = 0$; solid lines) and flow accumulation ($c_{FL} = 0.018$; dashed lines) for experiment lek2: a) Spatial distribution of stream power per unit length D_f [W m^{-1}]; b) Spatial distribution stream power per unit area $D_{f,A}$ [W m^{-2}]; c) Spatial distribution of erosion force τ**~~
995

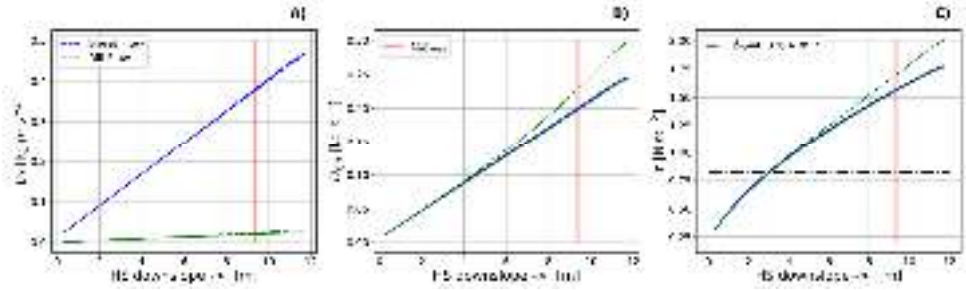

Figure 14: Results of CATFLOW-RILL for no flow accumulation ($c_{FL} = 0$; solid lines) and flow accumulation ($c_{FL} = 0.018$; dashed lines) for experiment oek2_4: a) Spatial distribution of stream power per unit length D_t [W m^{-1}]; b) Spatial distribution stream power per unit area $D_{t,A}$ [W m^{-2}]; c) Spatial distribution of erosion force τ

4.3.4 Energetic maxima and turbulent flow

As energy is additive, we can sum the potential and kinetic energy of rill- and sheet domain and compute the total free energy $E_{tot}^{HS} = E_{tot}^{SF} + E_{tot}^{RF}$ which is stored on the hillslope during steady state conditions (Fig. 15a). Like for the individual results of sheet- and rill flow (Fig. 13 and Fig. 14), total energy principally consists of potential energy. For the simulations of both experiments we observe a local maximum of E_{tot} in space, which manifests for oek2_4 farther downslope than for lek_2. The total amount of energy stored on the hillslope is larger for lek_2 than for oek2_4, mostly due to the increased water flow depth as a result of a larger friction coefficient. For oek2_4 the computation of surface runoff with Catflow-Rill has little effect as little to no significant rill flow has been observed during the experiment. For simulation of experiment lek_2, Catflow-Rill leads to less total energy which is stored on the hillslope and a shift of the local energy maximum in upslope direction.

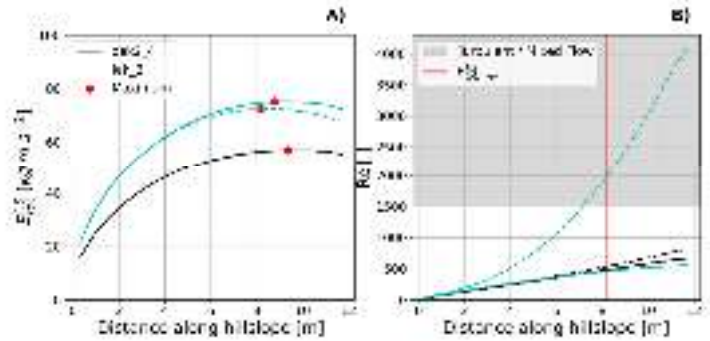

Figure 15: Results of CATFLOW (solid lines) and CATFLOW-RILL (dashed lines) for simulations of experiments oek2_4 (S=0.151 m m^{-1}) and lek_2 (S=0.163 m m^{-1}): a) Distribution of total free energy $E_{tot}^{HS} = E_{pot}^{HS} + E_{kin}^{HS}$ per unit flow length; b) Distribution of Reynolds number Re (Eq. 8)

For the analysis of flow regime, we plotted in Fig. 15b flow Reynolds numbers (Eq. 8) of each simulation as function of hillslope length. According to Emmett (1970), surface runoff is considered of laminar flow regime up to Reynolds numbers of 1500. Between 1500 and approximately 6000, the flow regime switches from laminar to mixed and turbulent flow. For simulations with sheet flow only, maximum flow Reynolds numbers stay below 1000 for the entire hillslope. The only simulation where flow Reynolds number exceeds the critical value of 1500 (grey shaded area) and increases up to 4000 is the one with rill domain for the experiment lek_2. Note that flow Reynolds number increases exponentially up to the location of the total energy maximum (red vertical line, Fig. 15b), and from there it grows linearly to hillslope toe.

5 Discussion

In this study we explore how potential energy and stream power of Hortonian surface runoff is controlled by macro- and micro-topography. To this end we establish a link between these controls and a thermodynamic perspective on conservation of energy and dissipation of free energy. As stream power is a flux of kinetic energy and therefore driven by energy gradients, we focus on the principal controls at the hillslopes scale namely the decline in geopotential, due to topography and the redistribution of water mass through flow accumulation. The analysis of typical hillslope forms, width functions and effective rainfall intensities revealed that the trade-off between mass accumulation and declining geopotential implies that potential energy of surface runoff does first increase downslope up to a maximum value and from there it declines. The location of this peak in potential energy of surface runoff changes with geopotential profile and width function of the hillslope. Interestingly, the most common hillslope forms in nature are those where the peak of energy is farther upslope (exponential distribution of geopotential, converging width) compared to hillslopes with negative exponential distribution of geopotential and diverging width. This suggests that hillslopes morphologically evolve in such a way that their distribution of energy in overland flow approaches more and more the configuration of a river system with a uniform energy expenditure along the flow path (Fig. 4; cf. second principle in Rodriguez-Iturbe et al., 1992). We included this evolution process in Fig. 4 by indicating the directions (small arrows) the distribution of E_{pot} would evolve to. Flow accumulation leads upslope to shorter flow path lengths with increase of E_{pot}, shifting the point of energy maximum upslope (blue arrow). Downslope of the energy maximum, gradients flatten (red arrows) whilst upslope energy accumulates (green arrows). We propose that this evolution process is controlled by flow accumulation, in the form of macro- and micro-topography and to the extent that flow regime is a direct result of these controls. To further corroborate this idea, we would need to analyse detailed data on morphological development of a hillslope and surface runoff, which was beyond the scope of this study.

Furthermore, our results show that potential energy maxima vanish in case of an increasing upslope runon, and the hillslope energetically resembles runoff behaviour of a river, which constantly expends energy. This is in line with what is observed in nature, as surface runoff increases, there will be a flow path length where topsoil is completely eroded and water flow is transported in a channel with a turbulent flow regime, marking a transitional behaviour of energy build-up on the hillslope, which is then used (dissipated) to transport material first within the rill system and then the stream channel. With increasing amount of runoff these channels extend farther upslope, effectively shortening flow path lengths of sheet flow (cf. Horton, 1945). The distribution of energy and its gradients along the flow path are the fuel of surface runoff and therefore stream power. Our results show that the distribution of geopotential gradients controls the distribution of stream power per unit length. Largest rates of energy expenditure are bound to highest differences in geopotential as only a small fraction of available potential energy is not dissipated and conserved as free energy (Loritz et al., 2019; Bagnold, 1966). In contrast, magnitude of stream power per unit area is controlled by flow accumulation of surface runoff. If the same amount of discharge flows down two hillslopes with equal slopes but different widths, stream power per unit area is larger for the hillslope with smaller width, also increasing the force that acts on bed material. Erosion and therefore the redistribution of geopotential is a direct result of flow accumulation, a factor which is often not accounted for in macroscopic erosion models (Scherer, 2007). There are few studies which attributed downslope hydraulic geometric relations to flow accumulation (Parsons et al., 1990), highlighting that concentration of flow not only leads to more discharge per unit area and therefore stream power but also less resistance to flow, effectively minimizing frictional losses.

On a micro-topographic level, we investigated the interplay between sheet- and rill flow for overland flow energy using data from rainfall-runoff simulation experiments. Therefore, we present a straightforward and successful numeric approach to separate surface runoff into sheet- and rill flow. Here we explored (i) whether maxima of potential energy do indeed emerge on the short 12m experimental plots, (ii) how rills control their spatial location and magnitude, and (iii) whether these maxima

are related to reported transitions of flow regime from laminar to turbulent flow on hillslopes, using our thermodynamic framework.

We found that observed total runoff and distinctions between rill and sheet flow velocities were well captured by calibrating the macroporosity factor to the former and the flow accumulation coefficient to match rill flow. We stress that these simulations reproduce velocities of measured sheet flow- and rill flow well, without adjusting roughness parameters. This result alone indicates that flow accumulation in rills is important for simulating surface runoff and to explain micro-topographic adaptations as well as that the straightforward open book conceptualisation of the rill system is feasible.

Distribution of potential energy along the flow path for all simulations exhibited indeed a clear maximum. However, the maximum for the experiment with stronger and faster rill flow (lek_2) occurs farther upslope than for the experiment with little to no rill flow (oek2_4). The Catflow-Rill simulation results show that for the rill domain the maximum potential energy is computed in close distance to flow Reynolds numbers in the range of 1800 to 2000 (Fig. 15b). Although the model computes runoff with the Manning-Strickler formula, which is defined for turbulent flow, roughness coefficients were adjusted during the measurement campaign (Gerlinger, 1996) to fit into this framework, independent of prevalent flow regime and averaged over the experiment plot. It is therefore likely that for areas of the experiments with laminar flow, deduced Manning's n is underestimated. This effect becomes less important the more flow accumulates along the flow path and hydraulic conditions approach mixed to turbulent flow. With this in mind, the peak of total energy should occur some distance farther upstream than is shown in Fig. 15 and therefore coincide for experiment lek_2 with the range of Reynolds numbers (~1500) where a flow regime transition is expected to occur (Emmett, 1970). This result indicates that laminar surface runoff is related to the downslope build-up of energy (energy added by flow accumulation > energy dissipated) and mixed/ turbulent flow to net dissipation (energy added by flow accumulation < energy dissipated), highlighting that the distribution of potential energy in space is related to flow regime and therefore also erosional processes (see Fig. 4).

Also, the reported critical values of Re by Emmett (1970) are higher than they are found by Phelps (1975) and were not discussed for influences of relative roughness $k_s = d_{sed}/d$. Phelps (1975) highlights that critical Reynolds numbers are lowered as relative roughness increases and he showed that critical Re can be as low as 400 for k_s=0.5. Therefore, we calculated the relative roughness for the Weiherbach experiments (lek_2 and oek2_4) and found that k_s stays for steady state conditions below 0.1. This justifies that the assumption of laminar to turbulent transition in the reported range by Emmett (1970) of approximately Re=1500 is valid for the here presented experiments.

These energy dynamics and the observed transition processes of flow regime and erosion fit well into our thermodynamic perspective. First, flow accumulation in rills shortens the flow paths with net increase of energy and lengthens the flow paths with net decrease of energy. In line with Fig. 3, our interpretation is that a hillslope which accumulates more flow in a rill is closer to a river system from an energetic point of view than a hillslope with little to no flow accumulation. Secondly, simulations of lek_2 with significant rill flow show that total kinetic energy of the rill flow domain approaches kinetic energy of the sheet flow domain in downslope direction. The same is observed for stream power distribution and is in line with maximum power principles, which state that maximum total power is achieved through equal distribution of power rates across space and time (Kleidon, 2016). We see in fact strong similarities to the maximum power theorem in electrical circuits, which states that maximum power transfer is achieved if the load resistance matches the source resistance. For our example the source resistance would be represented by the resistance to flow within the sheet flow domain and the load resistance is equal to the resistance to flow of the rill flow domain. As sheet- and rill flow domains of Catflow-Rill share the same slope, not only ratio of resistance to flow, but also ratio of stream power of both domains approaches unity in downslope direction (see Annex C for derivation). In this context we want to stress that the observed differences in rill- and sheet flow velocities (Scherer et al., 2012) were calibrated in Catflow-Rill using flow accumulation in rills only. We thus state that the irrigated hillslope stripe during steady state runoff approached a maximum power state in downslope flow direction as a unified system. We therefore believe that the separation of a planar surface into functional units of surface runoff is helpful to test these principles and find

~~spatial equilibria, such as they have been proclaimed to exist e.g., between different hillslopes (Emmet, 1970) or at river confluences (Howard, 1990). In this sense our results show that there might exist such an equilibrium between the sheet flow and the rill flow domain, with the latter functioning as the highway that delivers sediment to the outlet and the sheet flow area operating as the sediment production source. If any one of the two functional units on average produces or delivers more sediment, there would be an imbalance, which undoubtedly will result in adaptation of energy gradients through erosion and deposition until balance between particle detachment and transport is once more achieved. The limit between particle detachment and transport must be characterized by physical parameters such as the erosion resistance factor. In strictly fluvial systems such an equilibrium is expressed by the proportionality between discharge and loss of geopotential and in electrical circuits by Ohm's law (Rinaldo et al., 1998), an analogy which is also drawn to explain the development of natural systems through the maximum power theorem (Kleidon, 2016). From the calibrated simulation results of stream power and surface runoff velocity we computed average bed stresses per unit area and found that for experiment lek_2 the flow path length, where forces in the rill domain significantly deviate from average erosion forces in the sheet flow domain, is where average bed stresses exceed measured critical erosion forces. Therefore, for a given rainfall-runoff event, with flow in structured rills and on unstructured inter-rill areas, rilling happens in accordance to average soil physical characteristics, which distributes dissipation equally between functional units. The initiation of a rill is a highly debated research topic, but studies show that rilling and channelization of land surfaces is related to the transition of diffusive erosion processes to an advective erosion process (Smith and Bretherton, 1972; Tarboton et al., 1992). Smith (2010) argues that the advective transport is a result of water flow in direction of the energy gradient, but that diffusive transport is driven by topographic slope. In between he also distinguishes advection driven diffusive transport, which occurs when slope and energy gradient are not equal. Considering the resulting distributions of potential energy as shown in Fig. 4 and in relative terms in Fig. 3, we argue that formation of runoff, its flow regime and sediment transport mechanisms are directly related to the distribution of potential energy along the flow path. A downslope increase of potential energy of the flow should therefore be related to diffusive sediment transport and predominantly laminar flow regime. Contrarily, a decrease of potential energy of water flow and an energy gradient approaching topographic slope is related to advective transport and therefore rill initiation, eventually transitioning into a fully turbulent flow regime and capacity limited sediment transport.~~

~~**6 Summary and Conclusion**~~

5 Summary and Conclusion

In this study we linked well-known processes of ~~Hortonian~~ surface runoff (Shih and Yang, 2009~~)~~), and erosion (Kirkby, 1971; Beven, 1996) to thermodynamic principles (Kleidon, 2016~~). As the~~) and theories derived thereof (Leopold and Langbein, 1962; Rodriguez-Iturbe et al., 1992). The geomorphological development ~~and~~, surface runoff ~~affect each other, we believe it~~and the dominant erosion process co-evolve. We could show that an approach to ~~be particularly useful to~~ account for the energy conversion and dissipation rates ~~for~~is a helpful unifying concept. ~~This~~ The core of this concept ~~includes the conversion of free energy into heat and therefore enables us to state three~~ are the residuals of the observable, free energy fluxes and particularly their spatial distribution, which is key to evaluate empirical friction laws of surface runoff velocities in a thermodynamic framework. Although we do not provide a full closure of the energy balance of surface runoff, we were able to test and corroborate two hypotheses about the distribution of ~~geopotential gradients which are the drivers of dissipation.~~ potential and kinetic energy of surface runoff and the related transition from laminar to turbulent flow, on two related hillslope scales. Hypothesis one states that surface runoff systems can be separated into an area of production- and an area of depletion of energy. Our second hypothesis relates the typical transitioning of flow (laminar to turbulent) and erosion (diffusive to advective type) regime to these zones.

Formatted: Highlight

~~First, in~~In line with our ~~analysis~~first hypothesis, we ~~show~~showed that hillslopes as mass-accumulating systems are characterized by a ~~distinctly different energetic behaviour in comparison to runon systems. The latter, e.g., a river does not necessarily lead to energetic maxima in space. When mass accumulation overweighs runon, which is usually the case for hillslopes, we will observe spatial maxima of potential energy. For these systems, a trade-off between~~ distinct energetic behaviour: The trade-off between downslope mass gain and geopotential loss along a runoff flow path leads to ~~energy maxima in space. Our results show that these maxima exist on hillslopes and therefore confirm hypothesis one. Then, referring~~a maximum of potential energy. We found that the location and magnitude of this maximum is a function of hillslope form and accumulated surface runoff. Specifically, we analysed the influence of typical hillslope macro-topographical profiles with a fixed accumulated runoff for the spatial pattern of overland flow energy. We found that hillslope forms which relate to diffusive erosion processes (soil creep SC) have an energetic maximum located farther downslope than hillslope profiles related to advective erosion (soil wash SW). One might therefore be inclined to relate maximum dissipation rates to the former hillslope type SC as for our example more energy is depleted on a shorter flow path. However, in relative terms we see that SW forms have much larger dissipation rates than RS or SC forms, implying that dissipation is increased and even maximized as relative dissipation per unit flow path is close to unity. At the same time, SW forms also increase kinetic energy per influx energy, a criterium proposed by various authors for maximization of power (Kleidon et al., 2013) as well as maximum entropy production (Leopold and Langbein, 1962).

Referring to our second hypothesis, we interpret ~~this finding~~these findings as ~~a result~~results of the ~~transitions~~transition of ~~prevalent dissipation processes~~dominant energy conversion process of ~~Hortonian~~ surface runoff. Hereby we present a ~~reasonable~~ theory why laminar flow regime should be related to sheet flow and mixed / turbulent flow is related to concentrated flow in rills and channels. ~~For the presented experiments we show that the build-up of potential energy on hillslopes happens~~ For the second application of this study, we create an extension to the numerical model Catflow, which allows an adjustment of flow accumulation, by separating runoff into sheet and rill flow and dynamically linking both one dimensional flow domains. The calibration to observed rill and sheet flow velocities from rainfall simulation experiments in the Weiherbach catchments revealed distinct flow accumulation coefficients, which clearly relate to the distribution of kinetic energy of and the relative contribution to surface runoff from both domains. In fact, we showed that maximum relative dissipation rates are achieved when kinetic energy exports from both domains are equal. This can be interpreted as a maximum power state with minimum production of total kinetic energy and related experiments therefore result in minimum sediment concentrations.

For those experiments that reached an energetic steady state, our simulations show that the build-up of potential energy on hillslopes is likely to occur under laminar flow conditions, while decrease of potential energy along the flow path ~~is a functionality of~~ seems to be related to concentrated~~, turbulent rill flow. Hypothesis one and two feed into hypothesis three, which states that dominance of surface runoff processes with respect to dissipation is directed to distribute potential energy uniformly along the flow path. This means that within each~~ rill flow with *Re* reaching values which classify as mixed or turbulent flow regime. We evaluated the *Re* at the flow path distance with maximum free energy in the simulated rill domain and found that values range between 600 to 2300, which classifies as the beginning of mixed and turbulent flow, depending on relative roughness. Although the rill model is a simplification of surface runoff, the well-matched rill and sheet flow velocities suggest that the model captures both runoff processes effectively. The results therefore present a valid estimate of the onset of mixed and turbulent flow by relating flow concentration to the distribution of energy production and depletion zones along the hillslope. The measurements at hand are certainly not comprehensive enough to allow a final conclusion whether a maximum of free energy defines the onset of a turbulent flow regime, but specifically designed and carefully measured experiments might reveal further insight on this. We would like to stress that the theory presented here applies to conditions where erosion is predominantly driven by surface runoff and not limited by vegetational and geological controls.

Our final comment is aimed at the common picture of runoff as a fixed volume of ~~hillslope surface the same amount of free energy converts into heat. This theory necessarily leads to maximum entropy (Leopold and Langbein, 1962; Kleidon, 2016)~~

~~of the whole hillslope and for a mass accumulating system signifies that unit stream power is minimized along the flow path (Yang, 1976).~~water losing energy by friction (e.g., Bagnold, 1966). We think that we have shown that this picture should be revised because a loss of mean flow energy does not necessarily imply an equal increase in production of heat but can also be translated into velocity fluctuations of turbulence or lift and accelerate sediment particles. All this affects real dissipation rates and needs to be considered if one ever attempts to depart from empirical friction laws of channel flow for estimation of surface runoff on hillslopes.

~~The spatial distribution of energy is therefore directed to evolve towards a state of maximum entropy and uniform energy expenditure in space. A hillslope has several options to adjust the distribution of potential energy, which we distinguish into macro- and micro-topographic controls. For macro-topographic controls, an exponential distribution of geopotential and a converging width function leads to the largest flow path lengths with net free energy loss, which happens to be the prevalent three-dimensional hillslope form in nature and a result of long-term erosional adaptation (Kirkby, 1971). On a micro-topographic level, we analysed the formation of rills as the main adaptation mechanism to redistribute energy fluxes in space. We show that the formation itself is not necessarily decreasing total frictional dissipation but rather serves as a means of faster flow accumulation, therefore distributing more energy to the transport of sediment within the rill and less energy to erosion by surface runoff. We found evidence that steady state runoff on the hillslopes developed to a maximum power state, where power is equally distributed in sheet and rill flow. In case this finding is corroborated within other experiments, it has important implications for constraining the control volume resistance of the rill system using optimality approaches.~~

Author contribution

S. Schroers conceptualized, implemented the ~~CATFLOW-RILL~~Catflow-Rill extension, conducted the analysis and wrote the paper. O. Eiff conceptualized and supervised the hydraulic concepts. A. Kleidon reviewed and edited the thermodynamic concepts. U. Scherer provided the original ~~CATFLOW~~Catflow setups and commented on surface runoff dynamics. J. Wienhöfer contributed to paper writing and ~~CATFLOW~~Catflow modeling. E. Zehe oversaw the study and theory development as mentor.

Competing interests

The authors declare that they have no conflict of interest.

References

Abrahams, A. D.; Parsons, J. D.; Wainwright, J. (1994): Resistance to overland flow on semiarid grassland and shrubland hillslopes, Walnut Gulch, southern Arizona. In: Journal of Hydrology (156), S. 431–446.

Abrahams, A. D.; Parsons, A. J.; Shiu-Hung, L. (1990): Field experiments on the resistance to overland flow on desert hillslopes. Erosion, Transport and Deposition Processes (189).

Abrahams, A. D.; Parsons, J. D.; Wainwright, J. (1994): Resistance to overland flow on semiarid grassland and shrubland hillslopes, Walnut Gulch, southern Arizona. Journal of Hydrology (156), pp. 431–446.

Achten, ~~Wouter~~W. M. J.; Dondeyne, ~~Stefaan;~~S.; Mugogo, ~~Samweli;~~S.; Kafiriti, ~~Elly;~~E.; Poesen, ~~Jean;~~J.; Deckers, ~~Jozef;~~J.; Muys, ~~Bart~~B. (2008): Gully erosion in South Eastern Tanzania: spatial distribution and topographic thresholds. ~~In:~~ Zeit fur Geo 52 (2), ~~S.~~ pp. 225–235. DOI: 10.1127/0372-8854/2008/0052-0225.

Ali, M.; Sterk, G.; Seeger, M.; Boersema, M.; Peters, P. (2012): Effect of hydraulic parameters on sediment transport capacity in overland flow over erodible beds. Hydrol. Earth Syst. Sci. 16 (2), pp. 591–601. DOI: 10.5194/hess-16-591-2012.

Bagnold, R. A. (1966): An approach to the sediment transport problem from general physics. ~~In:~~ US. geol. Surv. Prof. Paper (422-I).

Bejan, A.; Lorente, S. (2010): The constructal law of design and evolution in nature. ~~In:~~ Philosophical transactions of the Royal Society of London. Series B, Biological sciences 365 (1545), ~~S.~~ pp. 1335–1347. DOI: 10.1098/rstb.2009.0302.

Berger, C.; Schulze, M.; Rieke-Zapp, D. H.; Schlunegger, F. (2010): Rill development and soil erosion: a laboratory study of slope and rainfall intensity. ~~In:~~ Earth. Surf. Process. Landforms (35), ~~S.~~ pp. 1456–1467.

Berkowitz, B.; Zehe, E. (2020): Surface water and groundwater: unifying conceptualization and quantification of the two "water worlds". ~~In:~~ Hydrol. Earth Syst. Sci. 24 (4), ~~S.~~ pp. 1831–1858. DOI: 10.5194/hess-24-1831-2020.

Beven, K. J. (1996): Equifinality and uncertainty in geomorphological modelling. The Scientific Nature of Geomorphology: Proceedings of the 27th Binghamton Symposium in Geomorphology.

Beven, K. J. (2004): Robert E. Horton's perceptual model of infiltration processes. Hydrol. Process. 18 (17), pp. 3447–3460. DOI: 10.1002/hyp.5740.

Dunne, T.; Black, R. D. (1970): An experimental investigation of runoff production in permeable soils. Water Resour. Res. ~~Charru, F.; Mouilleron, H.; Eiff, O. (2004): Erosion and deposition of particles on a bed sheared by a viscous flow. In: J. Fluid Mech. 519, S. 55–80. DOI: 10.1017/S0022112004001028.~~ 6 (2), pp. 478–490. DOI: 10.1029/WR006i002p00478.

Dunne, T.; Dietrich, W. E. (1980): Experimental investigation of Horton overland flow on tropical hillslopes. Part II: Hydraulic characteristics and hillslope hydrographs. ~~In:~~ Zeitschrift für Geomorphologie (Supplement Band 35), ~~S.~~ pp. 60–80.

Emmett, W. W. (1970): The Hydraulics of Overland Flow on Hillslopes. ~~In:~~ US. geol. Surv. Prof. Paper (662).

Engman, T. E. (1986): Roughness coefficients for routing surface runoff. ~~In:~~ Journal of Irrigation and Drainage Engineering (112), ~~S.~~ pp. 39–53.

Evans, R.; Taylor, J. (1995): Some methods of directly assessing water erosion of cultivated land - a comparison of measurements made on plots and in fields. ~~In:~~ Progress in Physical Geography (19), ~~S.~~ pp. 115–129.

Faulkner, Hazel (2008): Connectivity as a crucial determinant of badland morphology and evolution. ~~In:~~ Geomorphology 100 (1-2), ~~S.~~ pp. 91–103. DOI: 10.1016/j.geomorph.2007.04.039.

~~Favis-Mortlock, F.; Boardman, J.; Parsons, A. J.; Lascelles, B. (2000): Emergence and erosion: a model for rill initiation and development. In: Hydrol. Process. (14), S. 2173–2205.~~

Gerlinger, K. (1996): Erosionsprozesse auf Lössböden: Experimente und Modellierung. Dissertation.

Gomez, J. A.; Darboux, F.; Nearing, M. A. (2003): Development and evolution of rill networks under simulated rainfall. ~~In:~~ Water Resour. Res. (6).

Govers, G. (1992): Relationship between discharge, velocity and flow area for rills eroding loose, non-layered materials. Earth. Surf. Process. Landforms 17, pp. 515–528.

Govers, G.; Takken, I.; Helming, K. (2000): Soil roughness and overland flow. ~~In:~~ Agronomie (20), ~~S.~~ pp. 131–146. DOI: 10.1016/0304-1131(75)90001-6.

Graeff, T.; Zehe, E.; Reusser, D.; Lück, E.; Schröder, B.; Wenk, G. et al. (2009): Process identification through rejection of model structures in a mid-mountainous rural catchment: observations of rainfall-runoff response, geophysical conditions and model inter-comparison. ~~In:~~ Hydrol. Process. 23 (5), ~~S.~~ pp. 702–718. DOI: 10.1002/hyp.7171.

Hooshyar, M.; Bonetti, S.; Singh, A.; Foufoula-Georgiou, E.; Porporato, A. (2020): From turbulence to landscapes: Logarithmic mean profiles in bounded complex systems. Physical review. E 102 (3-1), p. 33107. DOI: 10.1103/PhysRevE.102.033107.

Horton, R. E. (1933): The role of infiltration on the hydrologic cycle. Transactions, American Geophysical Union.

Formatted: English (United Kingdom)

Formatted: German (Germany)

Formatted: German (Germany)

Formatted: English (United Kingdom)

Horton, R. E. (1945): Erosional development of streams and their drainage basins; Hydrophysical approach to quantitive morphology. In: Bulletin of the Geological Soc. of America (56), S. pp. 275–370.

Howard Alan D. (1990): Theoretical Model of Optimal Drainage Networks. In: Water Resour. Res. (9), S. pp. 2107–2117.

Ijjasz Vasquez, E. J.; Bras, R. L.; Rodriguez-Iturbe, I.; Rigon, R.; Rinaldo, A. (1993): Are river basins optimal channel networks? In: Advances in Water Resources (16), S. pp. 69–79.

Kirkby, M. J. (1971): Hillslope process-response models based in the continuity equation. In: Special Publication Institute of British Geographers (3), S. pp. 15–30.

Kleidon, A. (2016): Thermodynamic foundations of the Earth system. New York NY: Cambridge University Press.

Kleidon, A.; Renner, M.; Porada, P. (2014): Estimates of the climatological land surface energy and water balance derived from maximum convective power. Hydrol. Earth Syst. Sci. 18 (6), pp. 2201–2218. DOI: 10.5194/hess-18-2201-2014.

Kleidon, A.; Zehe, E.; Ehret, U.; Scherer, U. (2013): Thermodynamics, maximum power, and the dynamics of preferential river flow structures at the continental scale. In: Hydrol. Earth Syst. Sci. 17 (1), S. pp. 225–251. DOI: 10.5194/hess-17-225-2013.

Landesanstalt für Umwelt, Baden Württemberg (2011): Pegeldaten. Online verfügbar unter https://www.hvz.baden-wuerttemberg.de/, zuletzt geprüft am 19.07.2021.

Lawrence, D. S. L. (1997): Macroscale surface roughness and frictional resistance in overland flow. Earth. Surf. Process. Landforms 22, pp. 365–382.

Leopold, Luna B., Langbein, Walter B. (1962): The concept of entropy in landscape evolution. In: US. geol. Surv. Prof. Paper (500-A).

Loritz, R.; Hassler, S. K.; Jackisch, C.; Allroggen, N.; van Schaik, L.; Wienhöfer, J.; Zehe, E. (2017): Picturing and modeling catchments by representative hillslopes. In: Hydrol. Earth Syst. Sci. 21 (2), S. pp. 1225–1249. DOI: 10.5194/hess-21-1225-2017.

Loritz, R.; Kleidon, A.; Jackisch, C.; Westhoff, M.; Ehret, U.; Gupta, H.; Zehe, E. (2019): A topographic index explaining hydrological similarity by accounting for the joint controls of runoff formation. In: Hydrol. Earth Syst. Sci. 23 (9), S. 3807–3821. DOI: 10.5194/hess-23-3807-2019.

Mualem, Y. (1976): A new model for predicting the hydraulic conductivity of unsaturated porous media. In: Water Resour. Res. (12), S. pp. 513–522. DOI: 10.1029/WR012i003p00513.

Nearing, M. A.; Kimoto, A.; Nichols, M. H.; Ritchie, J. C. (2005): Spatial patterns of soil erosion and deposition in two small, semiarid watersheds. In: J. Geophys. Res. 110 (F4), n/a-n/a. DOI: 10.1029/2005JF000290.

Nearing, M. A.; Polyakov, V. O.; Nichols, M. H.; Hernandez, M.; Li, L.; Zhao, Y.; Armendariz, G. (2017): Slope–velocity equilibrium and evolution of surface roughness on a stony hillslope. In: Hydrol. Earth Syst. Sci. 21 (6), S. pp. 3221–3229. DOI: 10.5194/hess-21-3221-2017.

Paik, K.; Kumar, P. (2010): Optimality approaches to describe characteristic fluvial patterns on landscapes. In: Philosophical transactions of the Royal Society of London. Series B, Biological sciences 365 (1545), S. pp. 1387–1395. DOI: 10.1098/rstb.2009.0303.

Paltridge, G. W. (1979): Climate and thermodynamic systems of maximum dissipation. In: Nature 279 (5714), S. pp. 630–631. DOI: 10.1038/279630a0.

Parsons, A. J.; Abrahams, A. D.; Luk, S. H. (1990): Hydraulics of interrill overland flow on a semi-arid hillslope, Arizona. In: Journal of Hydrology (117), S. pp. 255–273.

Phelps, H. O. (1975): Friction coefficients for laminar sheet flow over rough surfaces. In: Proceedings of the Institution of Civil Engineers (59), S. pp. 21–41. DOI: 10.1680/iicep.1975.3840.

Rieke-Zapp, D. H.; Nearing, M. A. (2005): Slope shape effects on erosion: a laboratory study. In: Soil Sci. Soc. Am. J. (69), S. pp. 1463–1471.

Formatted: English (United Kingdom)

Formatted: English (United Kingdom)

Rinaldo, A.; Rodriguez-Iturbe, I.; Rigon, R. (1998): Channel networks. In: Annual Review of Earth and Planetary Sciences (26), S. 289–327. DOI: 10.1146/annurev.earth.26.1.289.

Rodriguez-Iturbe, I.; Marani, M.; Rigon, R.; Rinaldo, A. (1994): Self-organized river basin landscapes: Fractal and multifractal characteristics. In: Water Resour. Res. 30 (12), S. pp. 3531–3539. DOI: 10.1029/94WR01493.

Rodriguez-Iturbe, I.; Rinaldo, A.; Rigon, R.; Bras, R. L.; Marani, A.; Ijjasz-Vasquez, E. (1992): Energy dissipation, runoff production, and the threedimensional structure of river basins. In: Water Resour. Res. (4), S. pp. 1095–1103.

Schäfer, D. (1999): Bodenhydraulische Eigenschaften eines Kleineinzugsgebietes- Vergleich und Bewertung unterschiedlicher Verfahren. Dissertation.

Scherer, U.; Zehe, E.; Träbing, K.; Gerlinger, K. (2012): Prediction of soil detachment in agricultural loess catchments: Model development and parameterisation. In: CATENA 90, S. pp. 63–75. DOI: 10.1016/j.catena.2011.11.003.

Scherer, Ulrike (20072008): Prozessbasierte Modellierung der Bodenerosion in einer Lösslandschaft. Karlsruhe, Univ., Diss (Schriftenreihe SWW, 129).

Schierholz, I.; Schäfer, D.; Kolle, O. (2000): The Weiherbach data set: An experimental data set for pesticide model testing in the field scale. In: Agricultural Water Management (44), S. pp. 43–61. DOI: 10.1016/S0378-3774(99)00083-9.

Schlichting, Hermann; Gersten, Klaus (2017): Boundary-Layer Theory. Berlin, Heidelberg: Springer Berlin Heidelberg.

Schumm, S. A.; Harvey, M. D.; Watson, C. C. (1984): Incised Channels: Morphology, Dynamics and Control: Water Resources Publications.

Seibert, S.; Auerswald, K.; Fiener, P.; Disse, M.; Martin, W.; Haider, A. M.; Gerlinger, K.:. (2011): Surface runoff from arable land- a homogenized data base of 726 rainfall simulation experiments. CRC/TR32 Database (TR32DB). DOI: 10.1594/GFZ.TR32.2,\%00202011.

Shih, H. M.; Yang, C. T. (2009): Estimating overland flow erosion capacity using unit stream power. In: International Journal of Sediment Research 24 (1), S. pp. 46–62. DOI: 10.1016/S1001-6279(09)60015-9.

Singh, V. P. (2003): On the Theories of Hydraulic Geometry. In: International Journal of Sediment Research (18), S. pp. 196–218.

Singh, V. P.; Yang, C. T.; Deng, Z. Q. (2003): Downstream hydraulic geometry relations: 1. Theoretical development. In:Smart, Water Resour. Res. 39 (12). DOI: 10.1029/2003WR002484.

Smith, T. R. (2010): A theory for the emergence of channelized drainage. In: J. Geophys. Res. 115 (F2). DOI: 10.1029/2008JF001114.

Smith, T. R.; Bretherton, F. P. S. (1972): Stability and the conservation of massChannel networks. Advances in drainage basin evolution. In: Water Resour. Res.Hydroscience (8), S. 1506–1529. DOI: 10.1029/WR008i006p01506pp. 305-346.

Tarboton, D. G.; Bras, R. L.; Rodriguez-Iturbe, I. (1992): A physical basis for drainage density. In: Geomorphology 5 (1-2), S. 59–76. DOI: 10.1016/0169-555X(92)90058-V.

Tennekes, H.; Lumley, J. L. (1972): A first course in turbulence. Cambridge Mass.: MIT Press.

van Genuchten, M. T. (1980): A closed-form equation for predicting the hydraulic conductivity of unsaturated soils. In: Soil Sci. Soc. Am. J. (44), S. pp. 892–898. DOI: 10.2136/sssaj1980.03615995004400050002x.

Wooding, R. A. (1965): A hydraulic model for the catchment-stream problem. In: Journal of Hydrology (3), S. pp. 254–267. DOI: 10.1002/9781118925935.ch2.

Yang, C. T. (1971): Potential Energy and Stream Morphology. In: Water Resour. Res. (7), S. pp. 311–322.

Yang, C. T. (1976): Minimum Unit Stream Power and Fluvial Hydraulics. In: Journal of the Hydraulics Division (102).

Zehe, E.; Becker, R.; Bárdossy, A.; Plate, E. (2005): Uncertainty of simulated catchment runoff response in the presence of threshold processes: Role of initial soil moisture and precipitation. In: Journal of Hydrology 315 (1-4), S. pp. 183–202. DOI: 10.1016/j.jhydrol.2005.03.038.

Zehe, E.; Blöschl, G. (2004): Predictability of hydrologic response at the plot and catchment scales: Role of initial conditions. ~~In:~~ Water Resour. Res. 40 (10). DOI: 10.1029/2003WR002869.

Zehe, E.; Blume, T.; Blöschl, G. (2010): The principle of 'maximum energy dissipation': a novel thermodynamic perspective on rapid water flow in connected soil structures. ~~In:~~ Philosophical transactions of the Royal Society of London. Series B, Biological sciences 365 (1545), ~~S.~~ pp. 1377–1386. DOI: 10.1098/rstb.2009.0308.

Zehe, E.; Ehret, U.; Blume, T.; Kleidon, A.; Scherer, U.; Westhoff, M. (2013): A thermodynamic approach to link self-organization, preferential flow and rainfall–runoff behaviour. ~~In:~~ Hydrol. Earth Syst. Sci. 17 (11), ~~S.~~ pp. 4297–4322. DOI: 10.5194/hess-17-4297-2013.

Zehe, E.; Flühler, H. (2001a): Preferential transport of isoproturon at a plot scale and a field scale tile-drained site. ~~In:~~ Journal of Hydrology 247 (1-2), ~~S.~~ pp. 100–115. DOI: 10.1016/S0022-1694(01)00370-5.

Zehe, E.; Flühler, H. (2001b): Slope scale variation of flow patterns in soil profiles. ~~In:~~ Journal of Hydrology 247 (1-2), ~~S.~~ pp. 116–132. DOI: 10.1016/S0022-1694(01)00371-7.

Zehe, E.; Maurer, T.; Ihringer, J.; Plate, E. (2001): Modeling water flow and mass transport in a loess catchment. ~~In:~~ Physics and Chemistry of the Earth, Part B: Hydrology, Oceans and Atmosphere 26 (7-8), ~~S.~~ pp. 487–507. DOI: 10.1016/S1464-1909(01)00041-7.

Zehe, E.; Sivapalan, M. (2009): Threshold behaviour in hydrological systems as (human) geo-ecosystems: manifestations, controls, implications. ~~In:~~ Hydrol. Earth Syst. Sci. (13), ~~S.~~ pp. 1273–1297.

Zhang, Z.; Savenije, H. G. (2018): Thermodynamics of saline and fresh water mixing in estuaries. Earth Syst. Dynam. 9 (1), pp. 241–247. DOI: 10.5194/esd-9-241-2018.

Appendix A

Energy ~~flow~~flux between thermodynamic sub systems

For each OTS_{sub} we apply Eq. (4) where potential and kinetic energy of the system do not change with time, so that:

$$0 = J^{pe}_{f,net}(x) + J^{ke}_{f,net}(x) + J^{pe}_{Peff}(x) - D_f(x) \quad \text{(A1)}$$

For potential energy conversion we obtain:

$$\frac{dE^{\mathrm{pe}}_f(x)}{dt} = 0 = J^{pe}_{f,net}(x) + J^{pe}_{Peff}(x) - P_f(x)$$
$$J^{pe}_{f,net}(x) + J^{pe}_{Peff}(x) = P_f(x) \quad \text{(A2)}$$

While kinetic energy conversion is as follows:

$$\frac{dE^{ke}_f(x)}{dt} = 0 = P_f(x) - D_f(x) + J^{ke}_{f,net}(x)$$
$$P_f(x) = D_f(x) - J^{ke}_{f,net}(x) \quad \text{(A3)}$$

To relate the spatial distribution of energy with energy fluxes we recall that the downslope mass flux ~~$\vec{v}*m$~~ is associated with downslope flux of kinetic and potential energy. The net fluxes correspond to the divergence of the kinetic and potential energy flow. $J^{pe/ke}_f$ ~~[~~in watt~~]~~ is here defined as the advective energy flux, which is the product of specific energy E_{sp} ~~[~~in joule kg^{-1}~~]~~ and flow rate ~~$\rho * Q$ [ρQ in~~ kg s^{-1}~~].~~ As per definition of Eq. (4A4), $J_{f,net}$ is positive for a decrease of energy flux over the control volume and therefore has the opposite sign to change in energy:

$$J^{pe/ke}_{f,net} = -div\left(J^{pe/ke}_f(x)\right) \quad \text{(A4)}$$

$$J^{pe}_f = E^{pe}_{sp}(x~~) *~~)Q(x) = ~~g * h~~gh(x)~~ * \rho * Q~~\rho Q(x) \quad \text{(A5 a)}$$

$$J^{ke}_f = E^{ke}_{sp}(x~~) *~~)Q(x) = \frac{v(x)^2}{2}~~ * \rho * Q~~\rho Q(x) \quad \text{(A5 b)}$$

$$J^{pe}_{Peff}(x) = ~~\rho * P_{eff}(x) * g * h~~\rho I(x) g h(x)~~ * b(x)~~)/(3.6 \times 10^6) \quad \text{(A6)}$$

Inserting the expressions for specific potential and kinetic energy (Eq. (A5) to Eq. (A6)) into Eq. (A2) and Eq. (A3), we get power (Eq. (A7)) and dissipation (Eq. (A8)) of flow energy per unit length in ~~[~~W~~]~~watt m^{-1}~~].~~:

$$P_f(x) = J^{pe}_{f,net}(x) + J^{pe}_{Peff}(x)$$
$$= ~~\rho * g$$
$$~~ * \left(-\frac{dQ(x)}{dx} * h(x) - \frac{dh(x)}{dx} * Q(x) + P_{eff}(x) * h(x)$$
$$~~ * b(x)~~) \rho g \left(-\frac{dQ(x)}{dx} h(x) - \frac{dh(x)}{dx} Q(x) + P_{eff}(x) h(x) b(x) \right) \quad \text{(A7)}$$

Formatted: Font: Italic

Formatted: Font: Italic

$$
\begin{aligned}
D_f(x) &= P_f(x) + J_{f,net}^{ke}(x) \\
&= \cancel{\rho * g} \\
&\cancel{*\left(-\frac{dQ(x)}{dx} * h(x) - \frac{dh(x)}{dx} * Q(x) + P_{eff}(x) * h(x)\right.} \\
&\cancel{\left. * b(x)\right)} \rho g \left(-\frac{dQ(x)}{dx} h(x) - \frac{dh(x)}{dx} Q(x)\right. \\
&\left. + I(x) h(x) b(x) / (3.6 \times 10^6)\right) \quad - \frac{1}{2} \cancel{* \rho} \\
&\cancel{*\left(\frac{dQ(x)}{dx} * v(x)^2 + 2 * v(x) * \frac{dv(x)}{dx} * Q(x)\right)} \rho \left(\frac{dQ(x)}{dx} v(x)^2\right. \\
&\left. + 2v(x) \frac{dv(x)}{dx} Q(x)\right)
\end{aligned}
\tag{A8}
$$

Appendix B

~~**Run-off vs. run-on systems**~~

~~We now separate cases that accumulate runoff in downslope direction from cases with runon and transitory states (compare Fig. B1a, and Fig. B1b). In Fig. 6b we already plotted E_f^{pe} per unit length of all considered geopotential distributions z(x) with a constant width for a rainfall intensity of 50 mm hr^{-1} without runon (Q_0=0). Here, Fig. B1a represents the transition from a runoff only to a runon only system with a rainfall of 50 mm hr^{-1} and runon of 20 kg s^{-1}, while Fig. B1b shows the potential energy distribution for a runon only system without rainfall (I=0) and Q_0 of 20 kg s^{-1}.~~

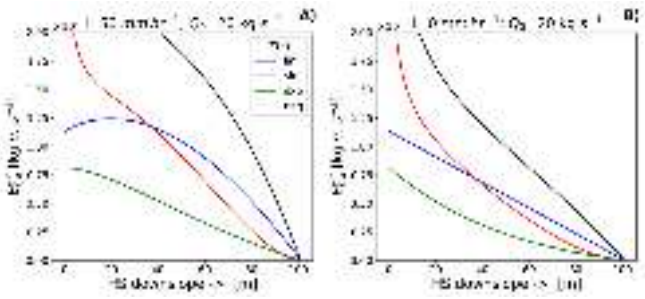

~~**Figure B1: Distribution of potential energy E_f^{pe} per unit length in [Joule m^{-1}] a) with runon and runoff accumulation and c) with runon but without runoff accumulation**~~

~~From these calculations, it appears that runoff accumulating systems show distinct energy conversion dynamics in comparison to runon systems, where runon outplays rainfall accumulation. Most strikingly, the accumulation of runoff in space energetically counteracts the depletion of geopotential gradients and leads to an energetic maximum. This stands in contrast to pure runon systems where energy is continuously depleted downslope. In between the two extremes, we observe transitions, which can result in local maxima, such as in the example of a linear slope (z_{lin}(x), Fig. B1a) depending on rainfall and runon intensities.~~

~~The unrealistically high potential energies for z_{sin}(x) and z_{neg}(x) (Fig. B1a, and Fig. B1b) within the first 20 meters of the hillslopes are due to our assumption that the energy gradient can be approximated by the slope of the terrain for the calculation of flow depth. The real energy gradient at these very small slopes cannot be approximated with slope and would require the solution of the momentum equation as e.g., in the shallow water equations in combination with proper upstream boundary conditions but is out of scope for this analysis.~~**Correlation of Manning's *n*, ratio of sheet to rill velocity, slope and C_f**

The Figures B1 to B4 are based on values derived from measurements (Manning's n, v_{RF}, v_{SF}, slope) and calibrated (C_f) values for all 31 analysed rainfall simulation experiments (cf. Gerlinger, 1996; supplemental data). Correlation was expressed by a power law which was fitted to mean bin values containing at least 2 values or more.

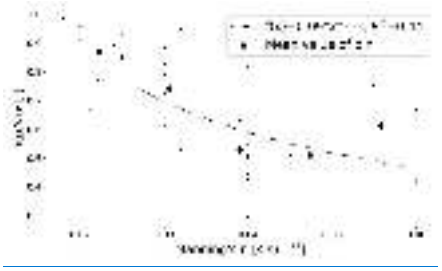

Figure B1: Manning's n vs. ratio of sheet to rill flow velocity

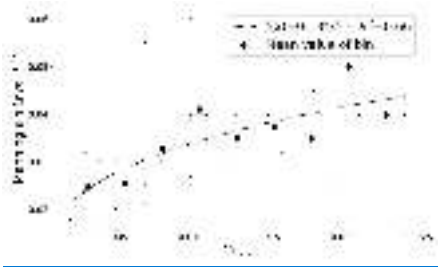

Figure B2: Calibrated flow accumulation C_f vs. Manning's n

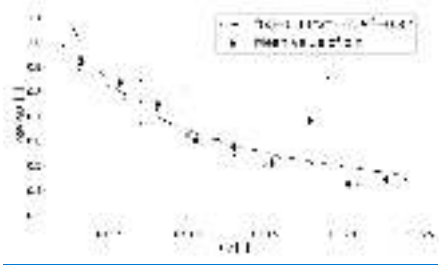

Figure B3: Calibrated flow accumulation C_f vs. ratio of sheet to rill flow velocity

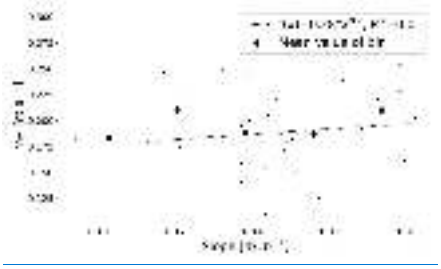

Figure B4: Slope of experiment plots vs. rill flow velocity

1420

Formatted: Indent: Left: 0 cm

Appendix C

Maximum Power in rill domain

Flow on hillslope equivalent to current in circuit:

	Hillslope	Electrical Circuit
Flow	$Q = K * S^{0.5}$	$I_{el} = \frac{1}{R_{el}} * V_{el}$
Power	$P = Q^2 * \frac{1}{K} * \rho * g$	$P_{el} = I_{el}^2 * R_{el}$

With

symbol	unit	description
I_{el}	[A]	Electrical current
R_{el}	[Ω]	Resistance
V_{el}	[V]	Voltage
P_{el}	[W]	External power of the electrical circuit
K	[$m^3 s^{-1}$]	Conveyance of the channel: $K = \frac{1}{n} * A * R^{\frac{2}{3}}$
R_K	[$m^{-3} s$]	Resistance to flow: $R_K = 1/K$

Therefore, channel conveyance is the inverse of the resistance of the channel to transport flow.

If water is mainly falling on sheet flow area and flows therefore first on sheet-flow area with R_K^{SF} and then accumulates in a channel with R_K^{RF} the total resistance to flow is:

$$R_K = R_K^{SF} + R_K^{RF} \tag{C1}$$

Here we assume that R_K^{SF} is fixed and that mainly resistance to flow of the rill adapts.

Total power in the rill is then:

$$P^{RF} = Q^2 * \frac{1}{R_K^{RF}} * \rho * g = \left(\left(R_K^{SF} + R_K^{RF}\right)^{-2} * S\right) * R_K^{RF} * \rho * g$$

$$= S * \rho * g \left(\underbrace{R_K^{RF} + 2 * R_K^{SF} + \frac{R_K^{SF\,2}}{R_K^{RF}}}_{T} \right)^{-1} \tag{C2}$$

C2 becomes maximum if the term "T" becomes minimum:

$$\frac{dT}{dR_K^{RF}} = 1 - \left(\frac{R_K^{SF}}{R_K^{RF}}\right)^2 \tag{C3}$$

The derivative (C3) becomes zero if:

$$R_K^{SF} = R_K^{RF}$$

Or equivalently:

$$K^{SF} = K^{RF}$$

Formatted: Font: Italic